Titre: Title:	Subharmonically pumped spatial waveguide array upconverter for high-power transmitters
Auteur: Author:	Jing Zhao
Date:	2003
Type:	Mémoire ou thèse / Dissertation or Thesis
Référence: Citation:	Zhao, J. (2003). Subharmonically pumped spatial waveguide array upconverter for high-power transmitters [Mémoire de maîtrise, École Polytechnique de Montréal]. PolyPublie. https://publications.polymtl.ca/7319/

Document en libre accès dans PolyPublie
Open Access document in PolyPublie

URL de PolyPublie: PolyPublie URL:	https://publications.polymtl.ca/7319/
Directeurs de recherche: Advisors:	Ke Wu
Programme: Program:	Non spécifié

UNIVERSITÉ DE MONTRÉAL

SUBHARMONICALLY PUMPED SPATIAL WAVEGUIDE ARRAY UPCONVERTER FOR HIGH-POWER TRANSMITTERS

JING ZHAO

DÉPARTEMENT DE GÉNIE ÉLECTRIQUE

ÉCOLE POLYTECHNIQUE DE MONTRÉAL

MÉMOIRE PRÉSENTÉ EN VUE DE L'OBTENTION
DU DIPLÔME DE MAITRISE ÈS SCIENCES APPLIQUÉES
(GÉNIE ÉLECTRIQUE)
JULY 2003

National Library
of Canada

Bibliothèque nationale
du Canada

Acquisitions and
Bibliographic Services

Acquisisitons et
services bibliographiques

395 Wellington Street
Ottawa ON K1A 0N4
Canada

395, rue Wellington
Ottawa ON K1A 0N4
Canada

The author has granted a non-exclusive licence allowing the National Library of Canada to reproduce, loan, distribute or sell copies of this thesis in microform, paper or electronic formats.

L'auteur a accordé une licence non exclusive permettant à la Bibliothèque nationale du Canada de reproduire, prêter, distribuer ou vendre des copies de cette thèse sous la forme de microfiche/film, de reproduction sur papier ou sur format électronique.

The author retains ownership of the copyright in this thesis. Neither the thesis nor substantial extracts from it may be printed or otherwise reproduced without the author's permission.

L'auteur conserve la propriété du droit d'auteur qui protège cette thèse. Ni la thèse ni des extraits substantiels de celle-ci ne doivent être imprimés ou aturement reproduits sans son autorisation.

In compliance with the Canadian Privacy Act some supporting forms may have been removed from this dissertation.

Conformément à la loi canadienne sur la protection de la vie privée, quelques formulaires secondaires ont été enlevés de ce manuscrit.

While these forms may be included in the document page count, their removal does not represent any loss of content from the dissertation.

Bien que ces formulaires aient inclus dans la pagination, il n'y aura aucun contenu manquant.

Canadä

UNIVERSITÉ DE MONTRÉAL

ÉCOLE POLYTECHNIQUE DE MONTRÉAL

Ce mémoire Intitulé :

SUBHARMONICALLY PUMPED SPATIAL WAVEGUIDE
ARRAY UPCONVERTER FOR HIGH-POWER TRANSMITTERS

Présenté par : Zhao Jing

En vue de l'obtention du diplôme de : Maîtrise ès Sciences Appliquées

a été dûment accepté par le jury d'examen constitué de :

Renato G Bosisio, M.Sc.A., président

Wu Ke, Ph.D., membre et directeur de recherche

Tayeb Denidni, Ph.D., membre

ACKNOWLEDGEMENTS

I would like to warmly thank my director Professor Ke Wu, for providing the opportunity to join the great research group, for his invaluable guidance, encouragement and confidence in me from the beginning and throughout this project. I would also like to acknowledge Professor Renato G. Bosisio, Professor Cevdet Akyel, Professor Fadhel Ghannouchi and Professor Robert Paknys for their unforgettable teaching.

I am grateful to the laboratory support team. My sincere thanks go to Steve Dube, Gauthier Jules and Brassard Roch for the prototype fabrications, and also to Gagne Jean-Frederic, Mekki Belaid and Cassivi Yves for their valuable advice and help with measurements.

I would like to express my heartfelt thanks to the group members, especially to Coulibaly Yacouba, Duochuan Li, Xu Xin Yu and Yang Ping for many "quick questions" and helpful discussions along the way. I would like to thank Antonescu Traian for lots of friendly helps, working on Corel Draw and the French translation. Thanks also to Xu Jijun, Xiaoma Jiang, David Dousset and Serioja-Ovidiu Tatu.

A word of thanks must be given to my wife, Huifang Gu. Without her love and support I might not have attended study in microwave engineering. She has always been there for me since 1984.

Finally, I would like to thank my son, and my parents.

RÉSUMÉ

Afin d'obtenir une puissance de sortie et/ou un rendement de puissance plus élevé, les circuits de basse puissance doivent être connectés avec des structures combinatoires. Comparé aux structures combinatoires industrielles réalisées à l'aide des lignes de transmission, le schéma pour la combinaison de puissance spatiale offre un rendement de puissance RF amélioré en couplant les composants aux ondes ou modes en espace libre. D'ailleurs, le mélangeur équilibré est connu à posséder des avantages par rapport à sa variante qui utilise une seule diode, comme, par exemple: bonnes isolations RF-IF et LO-RF, la rejection du bruit AM et des réponses erronées causées par le LO. Les mélangeurs pompés par les sous-harmoniques (SH) offrent des avantages supplémentaires quand ils fonctionnent avec un oscillateur local (LO) à la moitié de la fréquence RF du signal. Ce fait-ci est particulièrement attractif aux fréquences micro-ondes ou le coût de la puissance, ainsi que le bruit du LO augmentent rapidement avec la fréquence. Un mélangeur équilibré sous-harmoniques présente les avantages des mélangeurs pompés par les et des mélangeurs équilibrés si celui-ci est conçu d'une manière adéquate. Dans ce travail on présente une nouvelle architecture d'un convertisseur de sous-harmoniques en guide d'onde spatial pour la bande Ku. Ce type de convertisseur est capable de fournir une haute puissance à la sortie, sans les effets négatifs sur les pertes de conversion et la bande dynamique. On attend à obtenir une isolation augmentée entre les ports, bruit AM du LO réduit, ainsi qu'une charge diminue du LO. Cette nouvelle topologie peut aussi améliorer l'isolation entre les ports LO et RF grâce à la propriété coupe-bande du guide d'onde.

L'architecture moderne du convertisseur sous-harmoniques équilibré spatial en guide d'onde comprend plusieurs convertisseurs connectés en parallèle (quatre, dans notre cas). Chaque convertisseur est composé d'un convertisseur sous-harmoniques équilibré, et de deux transitions micro-ruban fente-ligne à ailette sur le même substrat. Les circuits sont

chargés symétriquement tout au long de la section transversale du guide d'onde. Les puissances RF et LO sont combinées et divisées dans l'espace.

Au début, on a conçu un translateur sous-harmoniques équilibré basé sur la technique micro-ruban. Il est optimisé à $2f_{LO}+f_{IF}$ pour pertes de conversion minimales et une gamme d'opération dynamique élevée. Dans la conception du translateur de fréquence on utilise un filtre passe-bas ainsi qu'un filtre passe-bande afin de séparer les signaux IF et RF. Ces deux filtres sont optimisés pour une fréquence de coupure de 3 GHz, une largeur de bande de 10% autour de 15 GHz. Leur conception a été vérifiée à l'aide des simulations EM, en utilisant le logiciel HP Momentum. Un anneau hybride est utilisé pour alimenter deux diodes connectés en antiparallèle avec le signal du LO en antiphase.

De plus, on a étudié deux transitions "micro-ruban"-"ligne-fente" et "ligne à ailette"-"guide d'onde" pour les trajets LO et RF. Les deux transitions sont optimisées à l'aide du logiciel commercial Agilent HFSS pour une réflexion minimale afin d'obtenir une bonne adaptation. Les résultats des simulations ont donné bonne performance, eu de pertes de réflexion moins que –26 dB autour de la fréquence LO de 7 GHz, et moins que –24 dB pour la gamme de fréquences RF de 14.5 a 15.4 GHz. La combinaison des deux transitions, microstrip-slotline-guide d'onde, produit une perte de réflexion moins que –25 dB autour de 7 GHz, et moins que –28 dB dans la bande de 14.5 a 15.4 GHz.

Finalement, le convertisseur utilisant un guide d'onde spatial a été construit et mesuré. Les résultats expérimentaux nous dévoilent des performances impressionnantes, pertes de conversion de 10.5 dB sur une bande de fréquence d'entrée entre 400 et 950 MHz. Il possède aussi une dynamique entrée/sortie très bonne (plus de 50 dB), ainsi qu'une linéarité accentuée: le point de compression 1-dB plus élevé que 3 dBm, le point d'interception de troisième ordre (IP3) plus élevé que 25 dBm pour une puissance LO de

15 dBm à la fréquence de 6.7 GHz. On a aussi mesuré une isolation de 78 dB entre LO et RF aux fréquences LO, une suppression des signaux-images de 17 dB, une excellente capacité de suppression de toutes les harmoniques d'ordre pair et des signaux parasites, ainsi qu'une efficacité augmentée pour la combinaison de puissance. La conception d'un convertisseur guide d'onde spatial peut être développé pour les émetteurs en ondes millimétriques sans amplificateurs.

ABSTRACT

In order to yield a higher power output and/or power added efficiency, low power solid-state power devices should be regrouped with combining structures. Compared with corporate combining structures based on transmission lines, the spatial power-combining scheme provides enhanced RF power efficiency by coupling the components to wave beams or modes in free space. On the other hand, the balanced mixer is known to have advantageous features over its single-diode counterpart, namely, good RF-to-IF and LO-to-RF isolations, and rejection of AM noise from the LO source and spurious responses. Subharmonically pumped (SH) mixer presents additional advantages when operating with an LO at ½ RF signal frequency. This is in particular attractive at millimeter-wave frequency where the cost of LO power budget and excessive LO noise increases rapidly with frequency. The balanced subharmonic mixer should possess the advantages of both subharmonically pumped and balanced mixers if the mixer design is made in an adequate manner. In this work, a novel architecture of a Ku-band spatial waveguide array balanced subharmonic upconverter is proposed for the first time. This kind of upconverter can provide more power output without adverse effects on conversion loss and input operating dynamic range. Higher isolation between ports, reduced LO AM noise and alleviated demand for LO source are expected. This new topology can also enhance the LO to RF port isolation by the cut-off nature of waveguide.

The novel architecture of a spatial waveguide array balanced subharmonic upconverter consists of multiple parallel upconverter unit cards (four cards in our experiments). Each of the upconverter unit cards is composed of a balanced subharmonic upconverter and two microstrip-slot-finline transitions on the same substrate. The unit cards are symmetrically loaded along the waveguide cross-section in an array form. The RF and LO powers are spatially combined and divided.

On the basis of the microstrip technique, a balanced subharmonic upconverter was designed at the beginning. It is optimized at $2f_{LO}+f_{IF}$ for minimum conversion loss and high operating dynamic range. In the upconverter design, a low-pass filter and a band-pass filter are used to separate IF and RF signals. With the insertion loss design method, the low-pass and the band-pass filters are optimized at a cutoff frequency of 3 GHz, and with a 10% bandwidth with respect to the center frequency of 15GHz, respectively. Their design was verified by EM simulation with the aid of commercial CAD software - HP ADS Momentum. A hybrid ring is used to provide two anti-parallel diode pairs with an 180° out-of phase and equal LO power level. A matching circuit is placed in front of two diode pairs at the side of RF/IF path due to a very low equivalent RF impedance presented by the anti-parallel diode pairs at RF frequency.

Moreover, two transitions of microstrip-to-slotline-to-finline-to-waveguide for both LO and RF paths are studied. With the help of commercial software Agilent HFSS, the two transitions are optimized for low return loss in achieving a good matching. Our EM simulated results show a very good performance with a return loss lower than –26 dB around the LO frequency of 7 GHz and lower than –24 dB over the RF frequency range of 14.5~15.4 GHz. The combination of the two transitions, microstrip-slotline-waveguide, yields a low return loss of less than –25 dB around 7 GHz and less than –28 dB over 14.5~15.5 GHz in the EM simulation.

Finally, the proposed spatial waveguide array upconverter is constructed and measured. It experimentally achieves an impressive performance that features a conversion loss lower than 10.5 dB over a large input IF frequency range of 400~950 MHz. It exhibits a very good dynamic input/output range (more than 50 dB) and a higher linearity: the input 1-dB compression point of higher than 3 dBm, the input third-order intercept point (IP3) of higher than 25 dBm under the 15.0 dBm LO driving at a fixed LO of 6.70 GHz. It also demonstrates 78 dB isolation between LO-to-RF at LO frequencies,

17 dB suppression of image signals, excellent suppression capability of all even-order harmonics and some other spurious signals, and higher power combining efficiency. The design approach of the spatial waveguide array upconverter could be further developed for the application of millimeter-wave front-end transmitter without power amplifiers.

CONDENSÉ EN FRANÇAIS

Comme les fréquences d'opération des composantes à semi-conducteurs ont augmenté jusqu'au niveau des ondes millimétriques, leur dimension, ainsi que leur puissance maximale dissipée ont diminué. Afin de pouvoir utiliser ces composantes pour des grandes puissances de sortie, ainsi que pour un rendement accru dans le domaine des ondes millimétriques, ceux-ci doivent être combinés.

Comparés aux structures combinatoires industrielles, bases sur des lignes de transmission, la combinaison des puissances fournit un rendement RF augmenté grâce au couplage des composantes aux faisceaux ou modes en espace libre, pas en utilisant des lignes de transmission. Si les composantes sont combinés par l'intermède des lignes de transmission, on a une limitation des nombre d'éléments causée par les pertes dans les lignes (dépendance non-linéaire). La complexité des circuits limite aussi le nombre des éléments. Pourtant, le rendement de l'architecture combinatoire ne varie pas avec le nombre d'éléments combinés, la seule limitation restant sa réalisation pratique. Récemment, on a réussi à obtenir des puissances ayant un niveau acceptable et un rendement de combinaison de 86%, tout en utilisant des éléments amplificateurs combinés spatialement [1]. Sans doute, on peut utiliser cette technique afin de combiner des oscillateurs, déphaseurs, mélangeurs et multiplicateurs de fréquence.

Aux fréquences millimétriques, il est difficile de concevoir une source LO et un amplificateur de puissance. On propose l'utilisation d'un réseau de convertisseurs en guide d'onde pour résoudre ce problème. La technique spatiale est utilisée pour combiner le signal du LO avec le signal RF. L'utilisation de cette méthode peut mener à une puissance de sortie augmentée, un rendement élevé sur une grande largeur de bande, tout en augmentant la plage d'opération dynamique et en réduisant la charge de la source LO. Cette structure sera très utile surtout aux fréquences millimétriques.

Le mélangeur est un circuit important du translateur de fréquence spatial. Il existent plusieurs types de mélangeurs, comme ceux pompés par sous-harmoniques, mélangeurs équilibrés et bout-singulaire. Le mélangeur pompé par sous-harmoniques est très utile dans le domaine des longueurs d'onde millimétriques grâce aux avantages du pompage sous-harmoniques et de la suppression du bruit AM du LO, ayant comme effet la diminution de la charge de la source LO. Le mélangeur équilibré est aussi utilisé grâce à sa capacité de mieux utiliser la puissance et sa rejection de certains signaux parasites, ainsi qu'une meilleure isolation LO/RF. Naturellement, le mélangeur équilibré à sous-harmoniques partage les avantages des mélangeurs SH et ceux de type équilibré.

Les caractéristiques I/V de la jonction d'une diode étant approximées par une série de puissances, nous pouvons démontrer les qualités des mélangeurs sous-harmoniques équilibrés : la suppression des harmoniques paires du RF et LO, les ordres paires (m et n sont impaires en $mf_{IF}+nf_{LO}$) et ordres impaires (m est pair et n est impaire) étant des signaux à mélanger. Nous obtenons la condition d'opération des mélangeurs équilibrés : deux paires de diodes en antiparallèle du circuit mélangeur SH doivent être alimentés par des signaux en opposition de phase avec le signal LO et en phase avec le signal IF.

Conception du Filtre

On utilise des filtres passe-bas et passe-bande afin de séparer le signal LO et le RF de signal IF. Comme résultat, les filtres sont fortement reliés aux performances du mélangeur pour obtenir de moindres pertes de conversion, haute isolation et distorsion réduite. Une procédure de conception, nommée "méthode de la perte d'insertion" utilise des techniques de synthétisation ou la réponse du filtre est rigoureusement définie. La conception est simplifiée si l'on commence par le filtre prototype passe-bas normalisé en termes d'impédance et de fréquence. On applique des transformations pour convertir le

prototype afin de le faire fonctionner dans la bande de fréquence et niveau d'impédance désirées. On obtient, à l'aide de la méthode des pertes d'insertion, un circuit primaire et on le simule et optimise à l'aide du logiciel HP-ADS.

On choisit la variante à trois sections afin de pouvoir obtenir une fréquence de coupure de 3 GHz et 30 dB d'atténuation à 7 GHz. Les valeurs des éléments du prototype sont : g_1=1, g_2=2, g_3=1 et g_4=1. On peut utiliser les transformations de Richard pour convertir les inductances et capacitances en lignes de transmission série ou parallèle, on applique la deuxième identité de Kuroda pour convertir les lignes série en lignes parallèle, et on calcule les impédances et les fréquences. Comme on utilise des lignes micro-ruban pour réaliser le filtre, les transformations de Richard servent à convertir les capacités shunt en lignes de transmission shunt et les inductances série en lignes série court-circuitées. L'inductance est remplacée par une ligne court-circuitée de longueur □l et impédance caractéristique L, en temps que la capacité soit remplacée par une ligne en circuit ouvert de longueur □l et impédance caractéristique 1/C. Les lignes série à la figure 2.2(b) sont très difficiles à réaliser en technologie micro-ruban. Pour contourner ce problème, on utilise les identités de Kuroda pour convertir les lignes série en lignes court-circuitées. On multiplie les impédances caractéristiques normalisées par 50 Ω et on choisit les longueurs des lignes à λ /8 à la fréquence 3 GHz. Le circuit est syntonisé et optimisé à l'aide du logiciel HP-ADS, puis vérifié par des simulations EM.

Le signal IF ayant une fréquence de 1 GHz, l'image RF aura la fréquence 13 GHz. Pour obtenir la rejection de l'image RF, ce filtre passe-bas doit posséder une atténuation d'au moins 20 dB dans la bande interdite, a une distance de 2 GHz de la fréquence centrale (f_0=15 GHz). On conçoit le filtre pour avoir aussi une réponse constante afin de maximiser les paramètres du mélangeur. On calcule les constantes J en tenant compte des valeurs des éléments du filtre prototype. Les impédances caractéristiques pour les modes

paire et impaire sont obtenues à l'aide des formules suivantes : $Z_{0e} = Z_0 [1 + JZ_0 + (JZ_0)^2]$ et $Z_{0o} = Z_0 [1 - JZ_0 + (JZ_0)^2]$. On obtient ainsi un circuit théorique à lignes couplées. Puis, on utilise le logiciel HP-ADS Momentum pour simuler et optimiser le circuit afin d'obtenir les meilleurs résultats possible. Les résultats de la simulation ADS Momentum montrent des pertes d'insertion de moins de 1dB à la fréquence centrale RF et plus de 16 dB de rejection aux fréquences-image. Le filtre est réalisé sur un substrat RT/Duroid® 6010LM ayant une épaisseur de 0.25 mm. Si l'on compare les résultats obtenus avec les simulations Momentum et ceux obtenus à l'aide de ADS, on peut remarquer la même largeur de bande, mais la fréquence centrale est décalée par 0.8 GHz. La perte d'insertion mesurée a une valeur de 0.5 dB plus grande que celle simulée. Ces différences peuvent être causées par la tolérance de la technologie de fabrication.

Translateur de Fréquences Sous-Harmoniques Equilibré dans la Bande Ku

Le translateur de fréquences qui utilise un réseau en guides d'onde, possède un faible bruit, pertes de conversion réduites, capacité de travailler en haute puissance, grande largeur de bande, haute isolation entre les ports, une moindre puissance nécessaire du LO, ainsi que des coûts de fabrication réduits. Comme un certain nombre de circuits translateurs de fréquence seront assemblés à l'intérieur du guide d'onde, il faut aussi prendre en considération la taille du circuit, la flexibilité du substrat, ainsi que la répétitivité des performances du circuit.

Il est très important de choisir le substrat qui correspond aux exigences avant de commencer la conception du circuit. Il faut prendre en considération les propriétés électriques et mécaniques du celui-ci. Une constante diélectrique élevée réduit les dimensions du circuit, mais introduit plus de pertes. Le substrat céramique Alumina peut être machiné à une précision élevée, mais il est beaucoup plus fragile que les substrats

mous. Finalement, on a choisit le substrat Rogers RT/Duroid® 6010LM, qui possède les caractéristiques suivantes : constante diélectrique élevée, qui se traduit par des dimensions de circuit diminuées, pertes réduites, en le prêtant pour le fonctionnement dans la bande Ku, hygroscopie réduite – qui ne modifie pas les pertes électriques, il est mou et flexible, ce qui nous permet de le couper en formes et dimensions désirées. Les données de catalogue de ce substrat sont : ε_r=10.2, h=10 mil, t=0.7 mil et tanδ=0.0023.

Les éléments actifs sont constitués par les diodes Schottky à Ga-As, modèle ALPHA DMK2308-000. Leurs performances sont excellentes, même si le prix est réduit. La capacitance de la jonction et la résistance série de la diode sont réduites, ainsi qu'une bonne caractéristique I/V. Les diodes connectées en antiparallèle possèdent des courbes I/V symétriques. Il est très important d'utiliser des diodes ayant caractéristiques identiques pour le mélangeur, cette condition sert à obtenir des pertes de conversion réduites, faible bruit, ainsi que la rejection de la deuxième harmonique et toutes les autres réponses parasites.

Le translateur de fréquence proposé contient cinq parties : un filtre passe-bande, un filtre passe-bas, un circuit d'adaptation, deux paires de diodes en antiparallèle et un circuit hybride en anneau. On a utilisé le même substrat (Rogers RT/duroid® 6010LM). Le filtre passe-bande est connecté au port RF et sert à l'extraction du signal RF. Il est utilisé pour laisser passer le signal $(2f_{LO}+f_{IF})$ d'une fréquence de 15 GHz, et fonctionne comme circuit ouvert pour le signal IF de 1GHz. Il rejette aussi le signal image $(2f_{LO}-f_{IF})$ de 13 GHz et d'autres signaux parasites. Le filtre passe-bas est connecté au port IF pour laisser passer le signal IF et de rejeter le signal RF, LO, le signal image, ainsi que les autres signaux parasites. Le circuit hybride en anneau est utilisé pour alimenter les deux paires de diodes avec des signaux LO d'amplitudes égales, en opposition de phase. Les amplitudes égales permettent aux paires de diodes de fonctionner en conditions optimales.

Les deux lignes en court-circuit sont localisées de côté LO des paires de diodes, d'une manière que celles-ci présentent un court-circuit pour la fréquence RF, mais que la fréquence LO soit moins affecté car celle-la est la moitié de la RF. Les lignes en court-circuit servent aussi comme circuit électrique vers la masse pour le DC et le IF. Le signal LO est divisé et déphasé à l'aide de l'anneau et les lignes série de longueurs $\square_{g,\,LO/2}$ qui mènent vers les deux paires de diodes. Le point de connexion entre les diodes deviendra ainsi une masse virtuelle à la fréquence LO pour l'excitation LO. Le circuit d'adaptation est conçu pour fournir une impédance d'adaptation optimale à la fréquence RF afin d'obtenir pertes de conversion minimales et une large bande dynamique. Normalement, il est difficile de réaliser un translateur pareil pour aboutir à une large bande dynamique, pertes de conversion réduites, puissance RF maximale à la sortie et pompage RF minimal à l'oscillateur local. Dans ce cas, il faut faire un compromis entre les résultats à obtenir durant le processus d'optimisation du circuit d'adaptation.

On utilise les modèles EM des circuits filtre passe-bande, hybride en anneau, circuit d'adaptation et filtre IF passe-bas qu'on trouve dans la bibliothèque du logiciel HP-ADS. Les paramètres simulés décrivent les propriétés des trois modèles de circuits d'une manière précise. Les paires de diodes sont crées par de modèles de jonctions non-linéaires trouvés dans la bibliothèque du logiciel ADS. On utilise l'instrument de simulation Balance Harmonique pour simuler le comportement du circuit, mais il faut prendre en considération les pertes additionnelles des circuits passifs pour obtenir des résultats qui valident le comportement réel des circuits.

Le circuit du mélangeur proposé est fabriqué sur un substrat 6010LM d'une épaisseur de 0.25 mm. On obtient de pertes de conversion de moins de 8 dB pour une bande de fréquences IF entre 720 et 1250 MHz, en utilisant une source LO a 6.75 GHz et une puissance fournie de 8.5 dBm. On obtient une perte de conversion de 6.6 dB à la fréquence de 900 MHz, ce qui est très proche de résultats des simulations. Le rapport

entre les pertes de conversion et le niveau de puissance IF à l'entrée est de 6.8 dB pour une large bande dynamique, la fréquence IF étant reglé à 0.9 GHz et la fréquence LO à 6.75 GHz. La puissance LO est 8.5 dBm et la puissance IF est balayé entre –50 dBm et 5 dBm. On obtient de pertes de conversion constantes en dessous d'une puissance IF de –10 dBm. Les pertes de conversion augmentent au-delà du niveau de –6 dBm de la puissance IF en raison de la saturation des diodes. Le point de compression mesuré se trouve à -4 dBm.

Réseau Spatial de Translateur en Guide d'Onde

L'architecture proposé est conçue comme un réseau spatial en guide d'onde dans lequel on trouve quatre circuits translateurs sous-harmoniques équilibrés. La fréquence LO étant la moitié de celle RF, on utilise deux guides d'onde pour les trajets LO et RF. On obtient ainsi une excellente isolation entre les ports RF et LO.

On a besoin d'utiliser de transitions micro-ruban à ligne à fente et ligne-ailette à guide d'onde afin d'alimenter chaque circuit du réseau spatial du translateur. Les transitions micro-ruban à ligne à fente et ligne-ailette à guide d'onde sont conçues d'une manière individuelle pour les fréquences RF et LO pour les deux trajets. Pour une transition micro-ruban à ligne à fente, la ligne à fente est constituée d'un espacement dans la couche conductrice laquelle est déposée d'un côté du substrat. La ligne est croisée perpendiculairement par un conducteur de l'autre côté du substrat. La ligne et la fente dépassent par un quart de longueur d'onde le point d'intersection entre la fente et le micro-ruban. Si l'on utilise le même substrat que celui pour le translateur équilibré sousharmoniques (Rogers RT/duroid® 6010LM), l'impédance minimale caractéristique de la ligne à fente Z_{0s} sera 90Ω et l'impédance caractéristique de la ligne micro-ruban Z_{0m} sera 62Ω à cause des tolérances de fabrication dans l'atelier du laboratoire. Cette situation

peut entraîner une limitation des valeurs Z_{0s} et Z_{0m} pour obtenir de pertes par réflexion réduites.

On modifie la configuration en introduisant un échelon dans la ligne micro-ruban. Cet échelon fonctionne comme un transformateur de réactance, il produit aussi une discontinuité au point d'intersection, celle-la réduisant d'une manière importante les pertes par réflexion sans diminuer la largeur de bande. Dans ce cas, on a besoin d'introduire un autre circuit d'adaptation. Ces deux structures de transition sont simulées et optimisées à l'aide du logiciel HFSS.

On utilise une ligne à ailette entre la ligne à fente et le guide d'onde rectangulaire, et la largeur de la ligne à fente est augmenté jusqu'à la largeur du guide d'onde afin de transformer graduellement l'impédance et d'éviter les réflexions. On introduit aussi une protrusion conique qui sert comme transformateur en quart de longueur d'onde pour réduire la discontinuité entre la ligne a ailette et le guide d'onde. Les dimensions de la ligne à ailette déterminent la fréquence centrale d'opération, ainsi que la largeur de bande dans le guide d'onde donne. Les structures de transition ligne à ailette – guide d'onde sont simulées et optimisées à l'aide du logiciel HFSS.

On utilise quatre circuits pour implanter le réseau de translateurs de fréquence. Ce nombre peut être augmenté. Ces circuits sont alimentés symétriquement au milieu du guide d'onde et sont équidistant à 2.28 mm. Chaque circuit est constitué d'un translateur équilibré à sous-harmoniques réalisé en technologie micro-ruban, une transition guide d'onde à micro-ruban pour le LO et une transition micro-ruban à guide d'onde pour le RF. On utilise le même substrat (Rogers RT/duroid® 6010LM) d'une épaisseur de 0.25 mm pour les intégrer.

Le réseau translateur en guide d'onde est pompé en utilisant un guide d'onde standard pour la bande C (WR-137). La puissance de l'oscillateur local est divisée spatialement à chaque port LO des mélangeurs et alimenté au translateur micro-ruban à l'aide des transitions guide d'onde – ligne à ailette et ligne à fente – ligne micro-ruban. Le signal RF de chaque mélangeur est combiné spatialement à l'aide d'un guide rectangulaire standard (WR-62) destiné pour la bande Ku. Le signal IF est appliqué par les connecteurs coaxiaux à la partie supérieure du guide WR-62. Le signal IF est divisé par un diviseur de puissance Wilkinson et transféré à chaque port IF des circuits.

On a fabriqué au début un seul circuit pour vérifier cette approche de conception et le fonctionnement du circuit. On a insèré le circuit mélangeur au milieu des guides d'onde WR-137 et WR-62. Les pertes de conversion étaient moindres que -8 dB$\pm$ 0.2 dB quand on a balayé le niveau du signal IF de -50 dBm à -10 dBm à une fréquence de 900 MHz, le signal du LO étant fixé à 6.75 GHz et une puissance de 8.5 dBm. Le point de compression 1-dB est plus élevé que -3 dBm, le point d'interception de troisième ordre IP3 est plus élevé que 11.3 dBm à la puissance de 15 dBm du LO pour la fréquence de 67 GHz.

Apres qu'on a obtenu de très bonnes performances en utilisant un seul circuit, on a crée un réseau de quatre circuits à l'intérieur du guide d'onde. La perte de conversion mesurée est de -10 dB pour une fréquence IF de 820 MHz, fréquence LO de 6.7 GHz à une puissance de 15 dBm. Cette perte de conversion excède de 1.5 dB celle du montage à un seul circuit. La cause pourrait être les fuites par radiation aux bouts du guide d'onde. Une autre explication serait que le champs électrique du mode TE_{10} produit un comportement différent à chaque circuit. Le point de compression 1-dB mesuré est plus élevé que 3 dBm. On remarque une amélioration de 6 dB par rapport au montage à un seul circuit. Les pertes de conversion restent constantes quand on modifie la puissance IF

entre −50 dBm et 0 dBm. On obtient aussi une meilleure linéarité, ainsi qu'un point de compression plus élevé.

Les résultats obtenus par des mesures nous démontrent pourquoi un réseau spatial de translateurs de fréquence peut fournir une meilleure efficacité RF en couplant plusieurs composants en faisceaux en espace, tout en obtenant une plage dynamique plus large au port d'entrée et une puissance de sortie plus grande. On obtient aussi une isolation de 78 dB entre les ports LO et RF aux fréquences LO, une suppression de 17 du signal-image, une efficacité augmenté pour combiner les puissances, ainsi qu'une capacité accrue de supprimer les harmoniques paires et les autres signaux parasites.

TABLE OF CONTENTS

LIST OF FIGURES

INTRODUCTION

As the operating frequency of semiconductor solid-state devices increases into the millimeter-wave region, the size of the devices and their power handling capability are reduced. In order to provide the advantages of a solid-state technology for achieving moderate/high power level output and/or power-added efficiency at millimeter-wave frequencies, solid-state components must be combined.

Compared with the corporate combining structures based on transmission lines, spatial power combining approach technically provides enhanced RF efficiency by coupling the components to beams or modes in free space rather than via transmission line scheme in the corporate combining structures. If the components are combined using transmission line circuits, there is an upper limit to the number of elements due to the inherent transmission line and combining structure losses that depend on the number of elements with a non-linear relation (equation) or due to an accumulating complexity of the circuit. However, the combining efficiency of the spatial combining architecture is constant with the number of elements combined, up to the physical limitation of the architecture. Recently, these techniques have already resulted in a number of successful demonstrations of spatially combined amplifier elements to reach useful power levels in frequency ranges from 10 GHz (150 watts) to 60 GHz (36 watts), and a combining efficiency of 86% has been obtained [1]. Undoubtedly, spatially combined arrays of other components, such as oscillator, phase shifters, mixers, and frequency multipliers, can also demonstrate their usefulness.

At millimeter-wave frequencies, it is difficult to design an excessive-power and stable LO source, and a high-power amplifier. To solve this bottleneck problem, we propose a spatial waveguide array upconverter in this work using a spatial technique in connection with LO power feeding and RF power combining as shown in Figure 1. This

can provide more power output with a constant high efficiency over a large bandwidth, and also increase operating dynamic range and reduce the demand for LO source. This structure will be very useful especially at millimeter wave and higher frequencies.
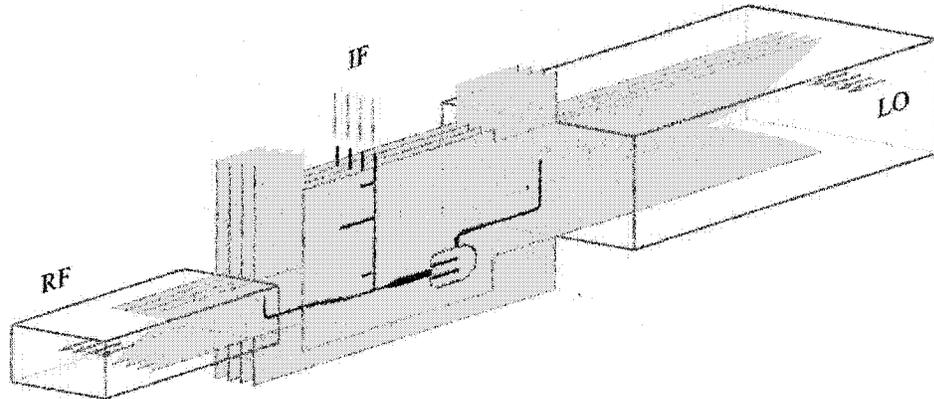

Figure 1. Spatial waveguide array power combining and dividing in the proposed upconverter architecture

Mixer is a key building block in the proposed spatial upconverter module. Generally speaking, there are several commonly used types of mixers, namely, subharmonically pumped mixer, balanced mixer, and single-end mixer. Subharmonically pumped (SH) mixer is very useful at millimeter wave frequencies because of its advantages of the subharmonic pumping and inherent local oscillator (LO) AM noise suppression, both alleviating demand for the LO source. The balanced mixer is also widely used due to its better power-handling capability and rejection of certain spurious signals as well as the enhancement of inherent LO-to-RF isolation. Of course, the balanced subharmonic mixer certainly shares the common advantages with both SH mixers and balanced mixers [2].

Obviously, our proposed new architecture can benefit the advantages of the subharmonic balanced mixer and the spatially waveguide array techniques. This is very important and attractive for millimeter-wave system design.

CHAPTER I

FUNDAMENTAL

1. FUNDAMENTAL

A spatial waveguide array upconverter consists of a number of frequency up converting mixers, microstrip-to-slot and finline-to-waveguide transitions. The mixer is therefore the key component in our project. Before staring our research project, it is important to know the basic mixer theory and to set up our design objectives.

1.1. Mixer Theory

Mixers are frequency conversion or translation devices. If it converts a signal from lower Intermediate Frequency (IF) to a high frequency (the RF frequency), it acts as an upconverter. Therefore, a down converter converts a signal from high frequency (the RF frequency) to a lower Intermediate Frequency (IF). Mixers can also be used as phase detectors and demodulators.

A mixer is fundamentally a multiplier. Figure 1.1 shows an ideal analog multiplier with two sinusoids applied to it. If the signal applied to the IF input port has frequency ω_i and the LO port has a frequency ω_p, through some trigonometric manipulation or calculation, the RF output will be found to consist of modulated components at the sum and difference frequencies. If there is a pass-band filter at RF port, we can get the desired frequency.
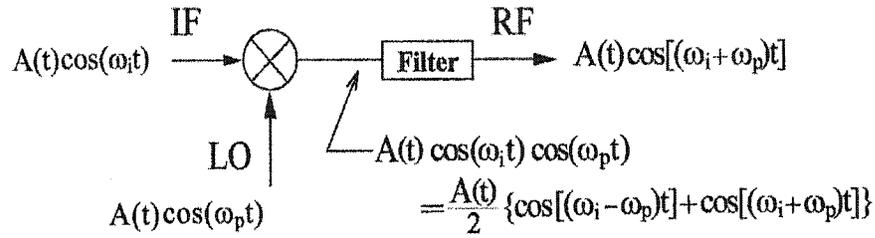
Figure 1.1   A mixer is fundamentally a multiplier.

Fortunately, an ideal multiplier is not the only thing that can realize a mixer. Any non-linear device can perform the multiplying function. The use of a non-ideal multiplier results in the generation of LO harmonics and in mixing products other than the desired one. The desired output frequency component can be filtered from the resulting mess.

The use of a non-ideal multiplier can be illustrated by describing the I/V characteristic of the non-linear device via a power series [2],

$$I = a_0 + a_1 V + a_2 V^2 + a_3 V^3 + \dots \qquad (1.1)$$

and letting V equal the sum of the two input in Figure 1.1. After an appreciable amount of algebraic and trigonometric manipulation, the output is found to be a signal having the original modulation, but shifted to the difference frequency. If it is assumed that the voltage of modulated input signal is much smaller than that of the LO, the current contains small-signal components at the frequencies

$$\omega_n = (\omega_i \pm \omega_p) + n\omega_p \qquad (n = 0, 1, 2, 3, \dots) \qquad (1.2)$$

again, by filter, it is generally easy to get the desired frequency signal.

1.2. Device for Mixers

Although, in theory, any non-linear or rectifying device can be used as a mixer, only a few devices satisfy the practical requirements of mixer operation. Any device used in a mixer must have a strong non-linearity, electrical properties that are uniform between individual devices, low noise, low distortion, and adequate frequency response.

The non-linear device most often employed for mixer is the Schottky-barrier diode, a diode consisting of a rectifying metal-to-semiconductor junction (Because frequency-response limitations imposed by recombination in the junction, *pn*-junction diodes are thoroughly unsuited for use in microwave mixers). Schottky-barrier diodes have lower junction capacitance and series resistance (two important parasitics), and a better *I/V* characteristic. Some high-quality Schottky-barrier diodes with diameters below 1 μm, have led to the development of practical mixers at frequencies above 1000 GHz. GaAs (Gallium Arsenide) is decidedly superior to silicon for high-frequency mixers because of its higher electron mobility and saturation velocity. These allow lower series resistance, for a specified junction capacitance, to be achieved in GaAs devices than in silicon. The performance of GaAs diodes regularly exceeds that of silicon, and reliability and damage resistance (because of GaAs diodes' higher breakdown voltages) are also superior. GaAs diodes are, however, significantly more expensive than silicon, and thus are normally reserved for more critical applications.

Field-effect transistor (FET) mixers have gained considerable popularly in recent years. Since they are better suited to MMICs than diodes: FETs do not require the non-

planar balun structures commonly required by balanced diode mixers, and they are compatible with the MMIC technology of FET amplifiers and other components (mixing diode and FET technology in a single chip often presents fabrication problems). Of course, a major advantage of FET mixers over diode mixers is the FET's ability to provide several decibels of conversion gain, while most diode mixers exhibit at least 5 to 6 dB of loss. FET mixers are regularly operated at frequencies extending well into the millimeter range; conversion gain has been achieved at frequencies above 90 GHz [2]. However, the FET usually needs a bias circuit that will increase the complexity of mixer.

In order to easily analyze and realize the upconverter, we select Schottky-barrier diodes as the mixing device in our project.

1.3. Schottky-Barrier Diode Model

In order to analyze mixers, it is necessary to have a circuit model of the Schottky-barrier diode that is valid for both large-signal and small-signal analyses.
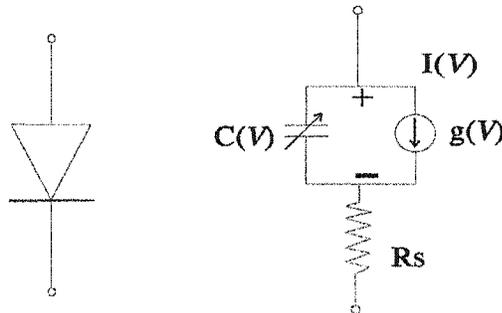

Figure 1.2   Equivalent circuit of a chip Schottky-barrier diode.

Figure 1.2 shows the equivalent circuit of a chip Schottky-barrier diode [2]. It consists of a non-linear conductance g(V) and capacitance C(V) representing the junction, and a series resistance Rs. Although the series resistance varies slightly with junction voltage, its non-linearity is usually negligible, and for virtually all purposes, it is treated as a linear element. The control voltage V is the junction voltage and it does not include the voltage drop across the series resistance Rs. Figure 1.2 also applies to both large and small signal analysis.

In a large signal analysis (such as calculating the LO waveforms in mixer), the capacitance C(V) and junction current I(V) are given by

$$C(V) = \frac{C_{j0}}{(1 - V/\phi_{bi})^{1/2}}$$
(1.3)

and

$$I(V) = I_0 \left(\exp(\frac{qV}{\eta KT}) - 1\right)$$
(1.4)

where C_{j0} is the zero-voltage junction capacitance and ϕ_{bi} is the junction's built-in voltage. I_0 is the reverse saturation current, q is the electron charge (1.6×10^{-19} coul), η is the ideality factor (usually less than 1.25), K is the Boltzmann's constant (1.37×10^{-23} J/K), T is the absolute temperature.

In small-signal analysis (which is used to determine the conversion loss), we linearize the I/V and C/V characteristics around the instantaneous large-signal voltage and treat the junction conductance and capacitance as linear, time-varying elements. This is justified by the factor that the RF and IF voltage components are small perturbations of the large-signal (LO) junction voltage. The small-signal junction conductance g(V) is the derivative of junction current with voltage:

$$g(V) = \frac{d}{dV} I(V) = \frac{q}{\eta KT} I_0 \exp(\frac{q}{\eta KT}) \qquad (1.5)$$

or

$$g(V) = \frac{q}{\eta KT}(I(V) + I_0) \qquad (1.6)$$

which gives that the junction conductance g(V) is proportional to its current I(V), because the reverse saturation current I_0 is very small compared to $I(V)$.

1.4. Basic Mixer Type

1.4.1. Balanced Mixer

Single diodes can be used as mixers (single-ended diode mixers), which have no inherent isolation between the mixer ports. However, the mixer designs more often use

combinations of two, four, or even eight devices in a balanced structure. Balanced mixers are loosely divided into two classes called single-balanced mixer and double-balanced mixers.

A single-balanced diode mixer uses two diodes. Either the LO drive or the RF signal is balanced (applied in anti-phase), adding destructively at the IF port of the mixer and providing inherent rejection. The level of rejection is dependent on the amplitude and phase balance of the balun, providing the balanced drive, and the matching between the two diodes. A rejection of 20 to 30dB is normally possible for good discrete designs. Other advantages of a single balanced design are rejection of certain mixer spurious products, depending on the exact configuration, and suppression of Amplitude Modulated (AM) LO noise. AM noise could be a significant problem in early microwave and mm-wave receivers where the available LO sources were very noisy. Modern wireless transceivers tend to make use of synthesized LO drives and the LO phase noise gives more of a problem than the AM noise.

Figure 1.3 shows a block diagram of a single balanced mixer. The LO drive to the two diodes is in anti-phase (balanced) and the RF signal is in-phase. If the mixing products are at $mf_{RF} \pm nf_{LO}$, this mixer will reject all products where m is even. If the RF drive were in anti-phase and the LO in-phase, all spurious products with n even would be rejected. The anti-phase signal is also cancelled at the IF port. Since the LO drive should be at a significantly higher level than the RF signal, it is often chosen as the anti-phase signal to increase the LO to IF isolation. However, it is also important to consider the spurious rejection properties. One disadvantage of balanced design is that they require a higher LO drive level.
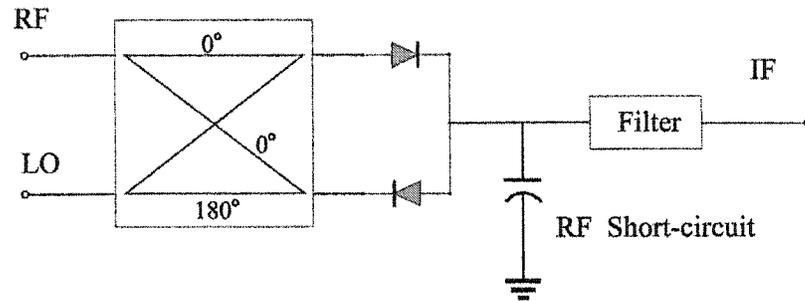
Figure 1.3. A block diagram of single balanced mixer

The RF short-circuit, shown at the IF port in Figure 1.3, is required for the mixer to function. Although shown explicitly here, it is normally incorporated in the IF low pass filter design. If the RF impedance at the IF port were high, the RF signal voltage across the diodes would be small and the mixer's conversion loss would be very high. The LO signal, however, does not require a low impedance at the IF port. Because the LO is a balanced signal across the diode pair, the common port of the diodes is a virtual earth to the LO. The LO drive across the two diodes adds destructively to a null at the common port, as if it were grounded. In most cases, however the LO and the RF are comparatively close in frequency and the RF short circuit will also be a good short circuit at the LO frequency.

A double-balanced mixer usually consists of four untuned devices interconnected by multiple hybrids, transformers, or baluns. The advantages of a double-balanced design over a single-balanced design are increased linearity, improved suppression of spurious products (all even order products of the LO and/or the RF are suppressed) and the inherent isolation between all ports. The disadvantages are that they require a higher level LO drive and require two baluns. Since they are too complicated to allow for individual tuning of the devices, so they may have higher conversion loss than a single-device or a single-balanced mixer.

1.4.2. Subharmonically Pumped Mixers

For many applications, it is expensive, inconvenient, or even impossible to generate a fundamental-frequency LO. The conversion loss and noise performance of a millimeter-wave mixer may be limited by the lack of adequate LO power or by excessive LO noise, rather than by the inherent capabilities of the mixer. In these cases, it may be wise to use a mixer that is pumped at half the LO frequency, and to mix the RF signal with the second harmonic of the junction's conductance waveform. Such subharmonically pumped mixers have remarkably good conversion performance, often only a decibel or two worse than comparable fundamental mixers. Even with greater conversion loss, a subharmonically pumped mixer often provides the best performance when all these other factors, especially LO noise and power, are considered.

It is possible to achieve subharmonic operation with a single-diode mixer. However, in such mixers the fundamental mixing response is usually greater than the second-harmonic response and is a source of interfering signals and down converted LO noise. It is also an additional loss mechanism, because a large fraction of the RF input power is converted to the mixing frequencies near the LO and radiated from the LO port. Unless the IF frequency is unusually high, it is impossible to filter out this response without rejecting the LO frequency as well. Hence, single-diode subharmonic mixers are rarely used.

Figure 1.4 is a circuit configuration, which can be used to realize a subharmonic diode mixer. For an LO input at $f_{LO}/2$, the output is maximized at $f_{LO}/2 \pm f_{RF}$ (or $f_{LO}/2 \pm f_{IF}$ when it is used as an upconverter).
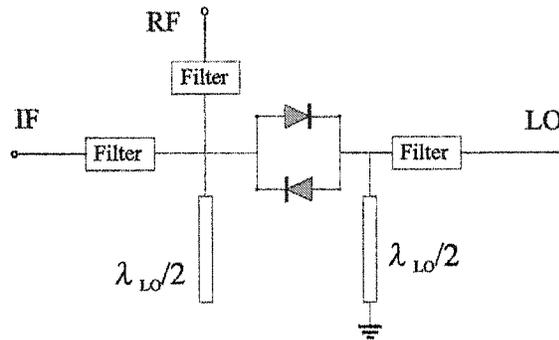
Figure 1.4. The basic configuration of a subharmonic mixer

The circuit makes use of an anti-parallel diode pair and provided the diodes are identical it has no fundamental mixing response. It also benefits from the fact that the f_{RF} and f_{LO} are normally relatively close in frequency (for a comparatively low IF). Thus the short circuit $\lambda_{LO}/2$ stub at the LO port is a quarter of a wavelength long at the input frequency of $f_{LO}/2$ and so is open circuit. However, at f_{RF} this stub is approximately a half wavelength long, so providing a short circuit to the RF signal. Conversely, at the RF input the open circuit $\lambda_{LO}/2$ stub presents a good open circuit to the RF but is a quarter wavelength long at the frequency $f_{LO}/2$ and so is short circuit. The IF is normally far enough away from the RF frequency to allow easy realization of an IF filter presenting an open circuit output to the RF port.

1.5. Design Objective

In most of millimeter-wave applications, the lowest possible conversion loss may not be required but a minimum LO power leakage at the RF port, less spurious responses and low noise as well as less demand on the LO source are expected. Combining the advantages of balanced and subharmonically pumped mixer schemes, our objective is to

design a balanced subharmonically pumped mixer for the development of a new spatial array upconverter.

CHAPTER II

FILTER DESIGN

2. FILTER DESIGN

2.1. Introduction

In mixers, low-pass and band-pass filters are used to separate the LO or RF signal from IF signal. As a result, filters are strongly relative with mixer performance in order to have a low conversion loss, high isolation and small distortion.

A design procedure, called insertion loss method [3], uses network synthesis techniques to design filters with a completely specified frequency response. The design is simplified by beginning with low-pass filter prototypes that are normalized in terms of impedance and frequency. Transformations are then applied to convert the prototype design to the desired frequency range and impedance level.

In this chapter, we start with the insertion loss method to get a primary circuit, and then we use the commercial software HP ADS to simulate and optimize the circuits for the targeted results.

2.2. Filter Design

There are two filters needed in a balanced subharmonic mixer. The one is low-pass filter to pass IF signal and reject all higher frequencies. The other is band-pass filter to extract RF signal.

2.2.1. Low-pass Filter

The low-pass filter is used to pass the IF signal which is around 1GHz, and prevent the leakage of LO, RF and mixing products from IF port. In order to achieve a wide band IF input and a good rejection of RF and LO frequencies, we design a maximally flat low-pass filter with cutoff frequency of 3 GHz, impedance of 50 Ω, and at least 30 dB insertion loss at RF frequency 7 GHz.

To determine the required order of the filter, the following expression is used to get the normalized frequency for the maximally flat filter prototype [3].

$$|\frac{\omega}{\omega_c}|-1 \tag{2.1}$$

Since the filter cutoff frequency $\frac{\omega_c}{2\pi} = 3.00\ GHz$ and attenuation frequency $\frac{\omega}{2\pi} = 7\ GHz$, then the normalized frequency for the maximally flat filter prototype is

$$|\frac{\omega}{\omega_c}|-1 = |\frac{7}{3}|-1 = 2.33 \tag{2.2}$$
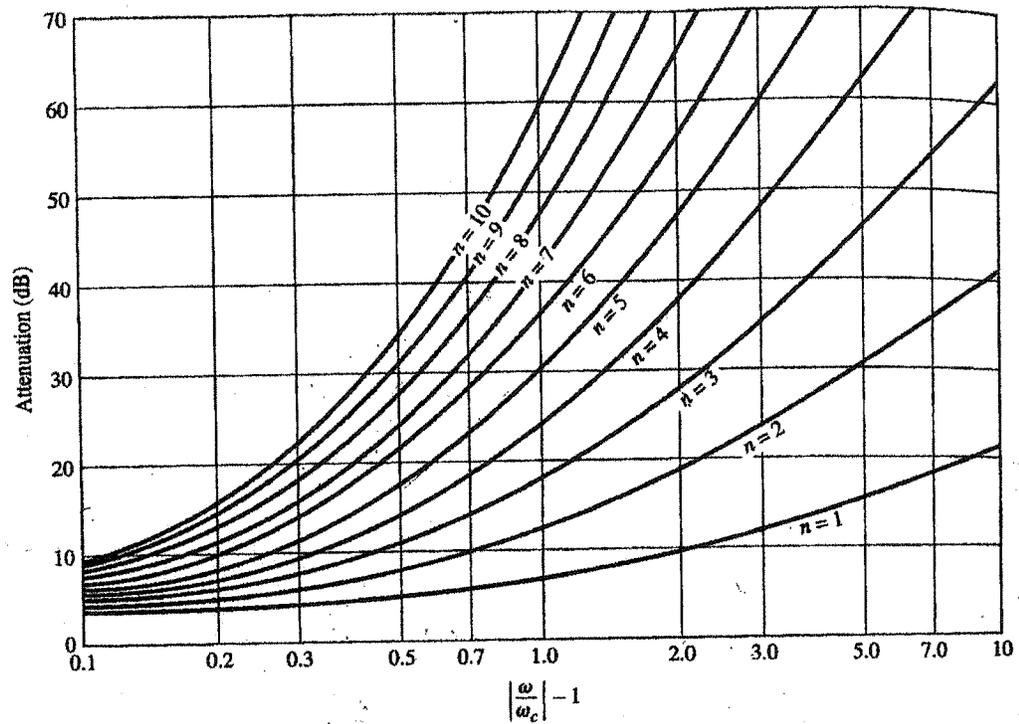
Figure 2.1. Attenuation versus normalized frequency for the maximally flat filter.

From Figure 2.1, we see that an attenuation of 30 dB at 7 GHz requires sections $N \geq 3$. We choose N=3, the corresponding low-pass filter prototype element values are [3]
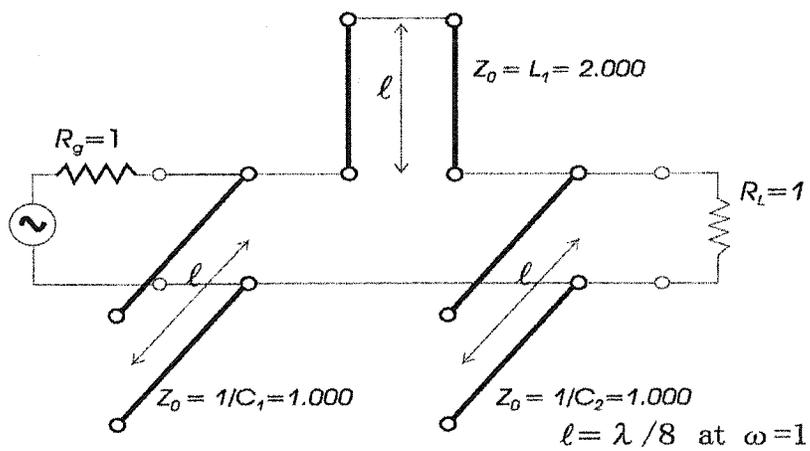
$g_1 = 1.0000 = C_1$; $g_2 = 2.0000 = L_1$;
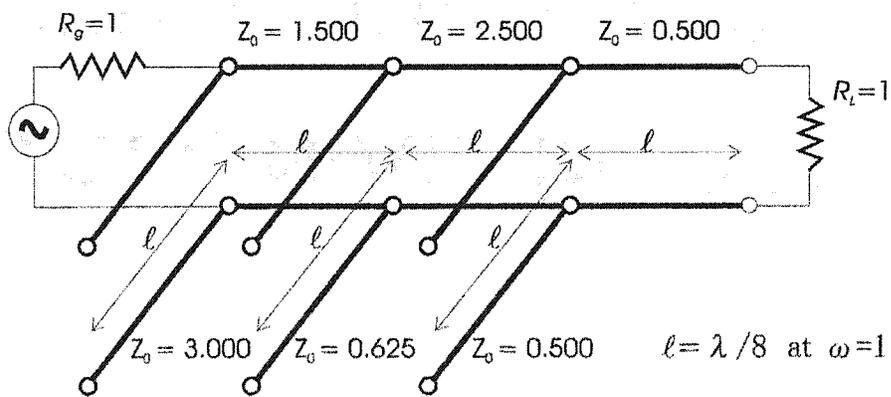
$g_3 = 1.0000 = C_2$; $g_4 = 1.0000 = R_L$

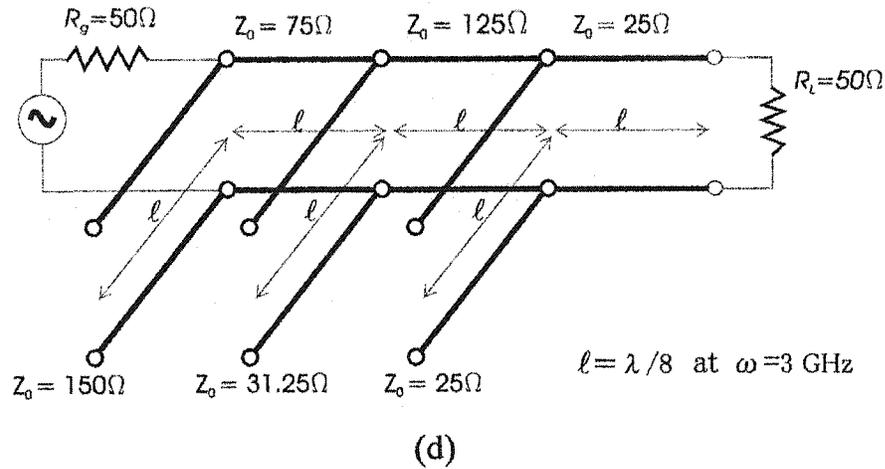with the prototype lumped-element circuit is shown in Figure 2.2(a).

(a)

(b)

(c)

$R_g{=}50\Omega$ $Z_0 = 75\Omega$ $Z_0 = 125\Omega$ $Z_0 = 25\Omega$

$R_L{=}50\Omega$

ℓ ℓ ℓ

ℓ ℓ ℓ

$Z_0 = 150\Omega$ $Z_0 = 31.25\Omega$ $Z_0 = 25\Omega$ $\ell = \lambda /8$ at $\omega =3$ GHz

(d)
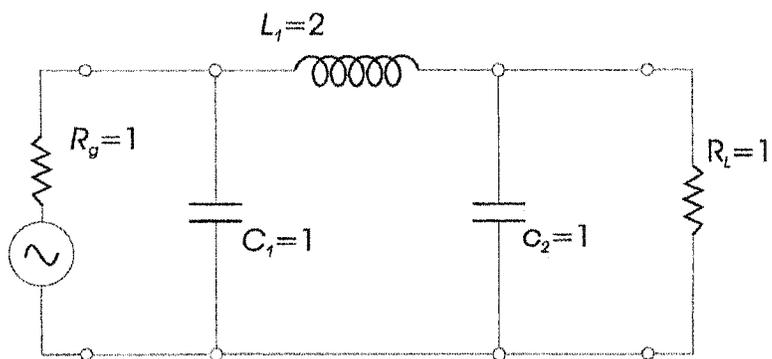
Figure 2.2. Filter design procedure. (a) Lumped-element low-pass filter prototype. (b) Using Richard's transformations to convert inductor and capacitors to series and shunt stubs. (c) Applying the second Kuroda identity to convert series stub to shunt stub. (d) After impedance and frequency scaling.

Since we use microstrip line to realize this filter, the Richard's transformations are used to convert shunt capacitors to shunt stubs and series inductors to series shorted stub, as shown in Figure 2.2(b). The inductor is replaced with a short-circuited stub of length $\beta\ell$ and characteristic impedance L, while a capacitor is replaced with an open-circuited stub of length $\beta\ell$ and characteristic impedance $1/C$.[3]

The series stubs of Figure 2.2(b) would be very difficult to implement in microstrip form, so we use Kuroda's identities to convert series stub to shunt stub, which is shown in Figure 2.2(c). Finally, we multiply the normalized characteristic impedances by 50Ω and choose the line and stub lengths to $\lambda /8$ at 3 GHz. The final circuit is shown in Figure 2.2(d).

Since the Rogers RT/Duroide® 6010LM has been chosen as the filter substrate, so the maximal characteristic impedance that can be realized is around 65Ω at frequency of design (the minimum width of microstrip is 5 mil). From Figure 2.2(d), we have the characteristic impedances of microstrip from 25Ω up to 125Ω, so it is still a problem for fabrication. However, the above analysis results can help us to build up a basic circuit, and then we use commercial software HP-ADS for designing a low-pass filter that carries out some tuning or optimization.

The final optimum design of low-pass filter is shown in Figure 2.3. It consists of three open stubs. The simulation results are shown in Figure 2.4. It has a very low insertion loss at 0-2 GHz and a pretty high rejection from 6 to 21GHz.
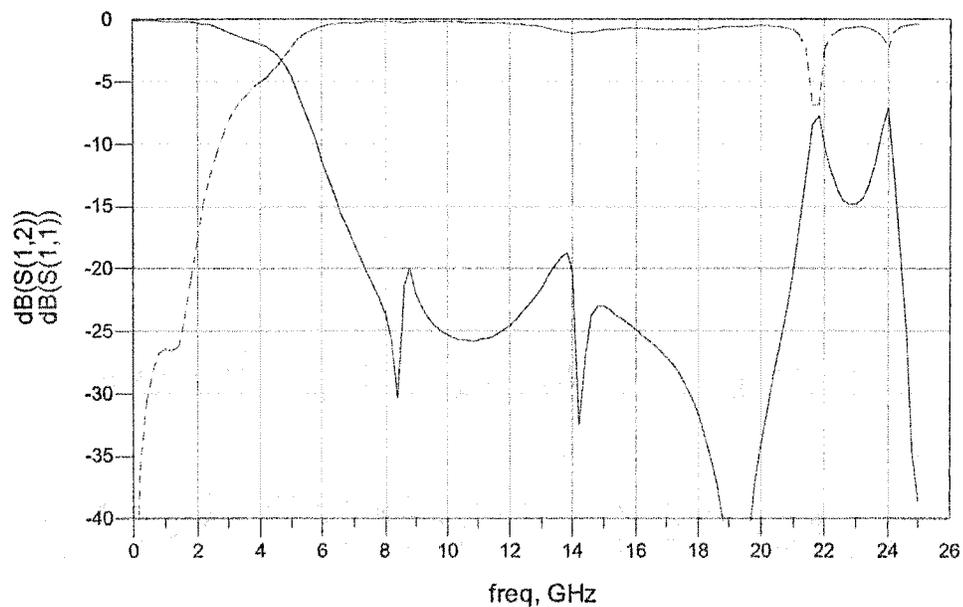
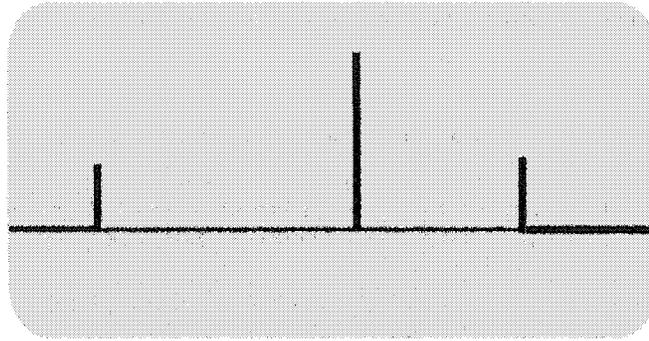Figure 2.3. Low-pass filter optimum simulation results.

Figure 2.4. The layout of low-pass filter

2.2.2. Band-pass Filter Design

The band-pass filter is used for RF signal (15GHz) extraction and also to reject LO, IF and certain spurious responses. The required center frequency f_0 is 15 GHz, and the fractional bandwidth is 10% (or $\Delta = 0.1$), and $Z_0 = 50\Omega$. Since the IF signal is around 1 GHz, the RF image will be 13 GHz. For rejection of the RF image, this band-pass filter must have at least 20 dB of attenuation in the stop band, 2 GHz away from the center frequency ($f_0 = 15$ GHz). We design the filter also with a maximally flat characteristic for obtaining a good conversion loss performance of the mixer.

First of all, we use the following frequency transformation to convert the band-pass filter design frequencies to the normalizes low-pass form ($\omega_c = 1$):

$$\omega \leftarrow \frac{1}{\Delta}(\frac{\omega}{\omega_0} - \frac{\omega_0}{\omega}) = \frac{1}{0.1}(\frac{13}{15} - \frac{15}{13}) = -2.87 \tag{2.3}$$

Then the value on the horizontal scale of Figure 2.1 is

$$|\frac{\omega}{\omega_c}| - 1 = |-2.87| - 1 = 1.87 \qquad (2.4)$$

which indicates an attenuation of at least 20 dB for N = 3.

The low-pass prototype values, g_n, are given in Table 2.1; then the following formula can be used to calculate the admittance inverter constants, J_n. [3]

$$Z_0 J_1 = \sqrt{\frac{\pi\Delta}{2g_1}}, \qquad (2.5)$$

$$Z_0 J_n = \frac{\pi\Delta}{2\sqrt{g_{n-1}g_n}}, \qquad \text{for } n = 2, 3, \ldots, N. \qquad (2.6)$$

$$Z_0 J_{N+1} = \sqrt{\frac{\pi\Delta}{2g_N g_{N+1}}}. \qquad (2.7)$$

Finally, the even- and odd-mode characteristic impedances can be found from:

$$Z_{0e} = Z_0 [1 + JZ_0 + (JZ_0)^2] \qquad (2.8a)$$

$$Z_{0o} = Z_0 \left[1 - JZ_0 + (JZ_0)^2\right] \qquad\qquad\qquad (2.8b)$$

All these results are summarized in the following table:

Table 2.1 Summary of band-pass filter design results

n	g_n	$Z_0 J_n$	Z_{0e} (Ω)	Z_{0o} (Ω)
1	1.5963	0.3137	70.61	39.24
2	1.0967	0.1187	56.64	44.77
3	1.5963	0.1187	56.64	44.77
4	1.0000	0.3137	70.61	39.24

Note that the filter sections are symmetric about the midpoint. Based on the theoretical design results, we use HP ADS momentum to simulate and optimize the circuit for the best possible design results.

The final optimum design of the band-pass filter consists of four coupled line sections. Figure 2.5 is the layout of this circuit. The ADS simulation results are shown in Figure 2.6, it has less than 1 dB insertion loss at center RF frequency and more than 16 dB rejection at image frequencies. Measured results are shown in Figure 2.7. That compare very well with the ADS simulated results, there is almost no change in filter bandwidth but the center frequency is shifted by 0.8 GHz. The measured insertion loss is 0.5 dB higher than the simulated value. Those differences may be caused by the fabrication tolerance.
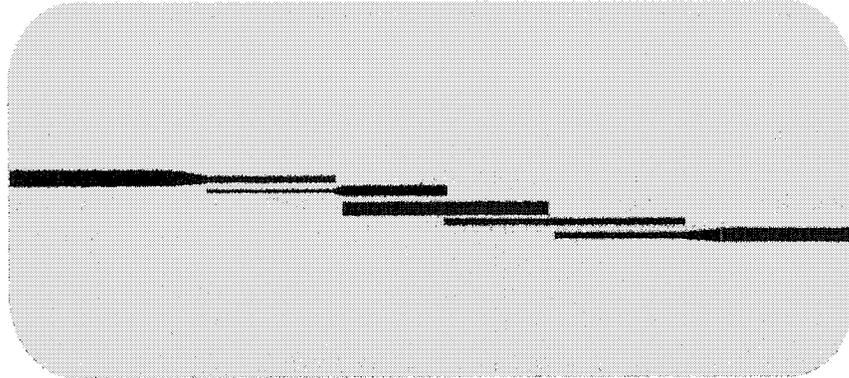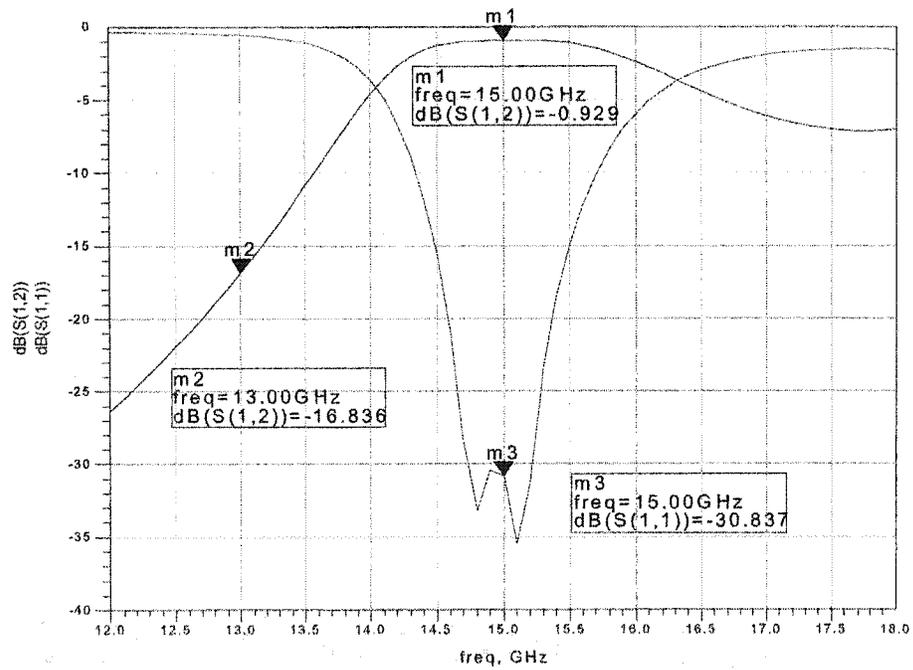
Figure 2.5 Band-pass filter layout.

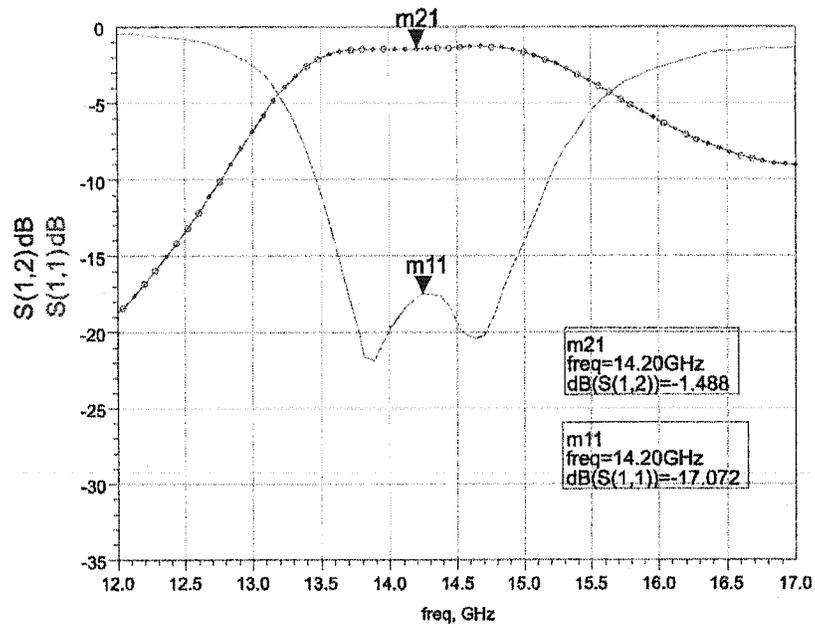Figure 2.6 Band-pass filter optimum simulation results.

Figure 2.7 Band-pass filter measured results.

2.3. Conclusion

Based on the insertion loss method, the two filters have been successfully designed for the application in our project of spatial array upconverter. The measured results show a good agreement as compared with the simulation results.

CHAPTER III

KU-BAND BALANCED SUBHARMONIC UPCONVERTER

3. KU-BAND BALANCED SUBHARMONIC UPCONVERTER

3.1. Introduction

The proposed Ku-band spatial waveguide array upconverter in microstrip format should have low conversion loss, low noise, large dynamic input/output range, more power handle ability, wide bandwidth, and high isolation between ports, less LO power demand and low fabrication cost. Since a number of Ku-band upconverter cards will be assembled in a waveguide in an array form, we also need to consider the circuit size, the flexibility of the circuit board, and the repeatable circuit performance.

As we described in Chapter I, the subharmonically pumped (SH) mixer is very useful at higher frequencies since it has the advantages of subharmonic pumping and inherent suppression of local oscillator (LO) noise, both alleviating the demand for the LO source. On the other hand, the balanced mixer is also widely used due to its rejection of certain spurious responses, its reduction of LO noise and spurious signals as well as its enhancement of inherent LO-to-RF isolation. Therefore, a balanced subharmonic mixer should be able to combine the advantages of both SH and balanced mixers if the mixer design is made in an adequate manner. In such mixers, anti-parallel diode pairs are used to replace single diodes, the LO is applied at ½ the frequency necessary to provide the desired frequency conversion, and the RF and IF are separated from each other by filters.

Since balanced subharmonic mixers share the common advantages with balanced mixer and subharmonically pumped mixers, it provides more flexibility of circuit design and high power-handling capability. In the meanwhile, less LO source demand is very useful in millimeter-wave or higher frequency applications. Several researchers have demonstrated the attractiveness of balanced subharmonic mixer performance [4].

In this chapter we will at first theoretically prove the inherent features of a balanced subharmonic mixer under the condition of the adequate excitation of the LO and RF signals. Next we will show the properties of substrate material and diodes that we choose in this design. Finally, a Ku-band balanced subharmonic upconverter will be presented with its optimal design and experimental results.

3.2. Features of the Balanced Subharmonic Mixer

In order to understand the mixer operation and extract the inherent features of balanced subharmonic mixers, we approximate the diode junction's I/V characteristic by power series [2] and derive useful results.
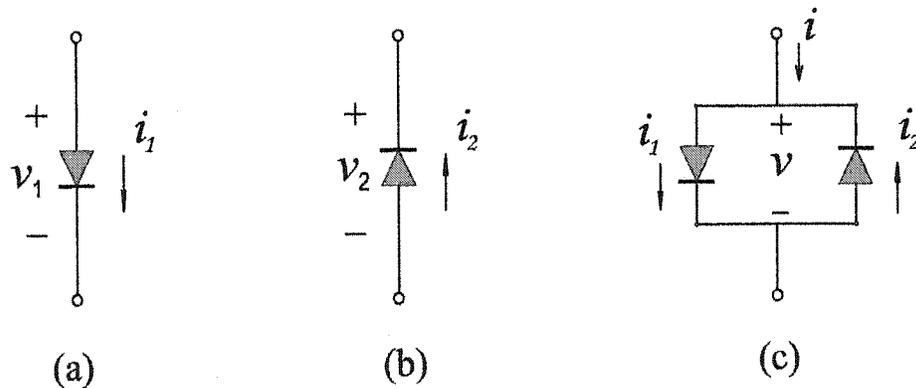
Figure 3.1 Currents and voltages in diodes.

In Figure 3.1 (a), the relation between the current and voltage is defined by:

$$i_1 = a_1 v_1 + a_2 v_1^2 + a_3 v_1^3 + a_4 v_1^4 + ... \qquad (3.1)$$

where v_1 is the total ac voltage across the diode (the RF plus the LO voltage), i_1 is the current, and a_k (k =1, 2, 3...) is constant. If the diode is reversed as shown in Figure 3.1 (b), only the applied voltage is reversed so the signs of the odd-power terms become negative:

$$i_2 = -a_1 v_2 + a_2 v_2^2 - a_3 v_2^3 + a_4 v_2^4 - ... \qquad (3.2)$$

From Figure 3.1 (c), the i current of an anti-parallel diode-pair is given by:

$$i = i_1 - i_2 = 2a_1 v + 2a_3 v^3 + 2a_5 v^5 + ... \qquad (3.3)$$

where v is the total ac voltage across the diode pair.

There are two diode-pairs in a balanced subharmonic mixer. The currents and voltages in the diode pairs of a balanced subharmonic mixer are shown in Figure 3.2.
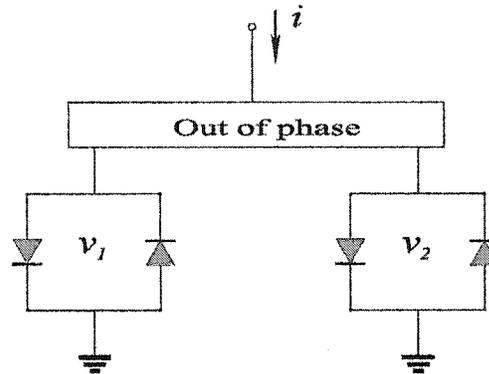
Figure 3.2. Current and voltages in a balanced subharmonic mixer

where v_1 and v_2 are ac voltages applied to the two diode-pairs respectively. Then, the i current is

$$i = a_1(v_1 + v_2) + a_2(v_1 + v_2)^2 + a_3(v_1 + v_2)^3 + a_4(v_1 + v_2)^4 + \ldots \qquad (3.4)$$

Considering the LO signal applied by $180°$ out-of-phase and the IF signal applied in-phase, respectively,

$$v_1 = -V_{LO}\cos(\omega_{LO}t) + V_{IF}\cos(\omega_{IF}t) \qquad (3.5)$$

and

$$v_2 = +V_{LO}\cos(\omega_{LO}t) + V_{IF}\cos(\omega_{IF}t) \qquad (3.6)$$

where V_{LO} and V_{IF} are the magnitudes of LO and IF signals, ω_{LO} and ω_{IF} are the frequencies of LO and IF signals respectively.

Substituting Equations (3.5) and (3.6) into (3. 4), we have,

$$i = a_1\left\{\left[-V_{LO}\cos(\omega_{LO}t) + V_{IF}\cos(\omega_{IF}t)\right] + \left[V_{LO}\cos(\omega_{LO}t) + V_{IF}(\omega_{IF}t)\right]\right\}$$

$$+ a_3\left\{\left[-V_{LO}\cos(\omega_{LO}t) + V_{IF}\cos(\omega_{IF}t)\right]^3 + \left[V_{LO}\cos(\omega_{LO}t) + V_{IF}(\omega_{IF}t)\right]^3\right\}$$

$$+ a_5\left\{\left[-V_{LO}\cos(\omega_{LO}t) + V_{IF}\cos(\omega_{IF}t)\right]^5 + \left[V_{LO}\cos(\omega_{LO}t) + V_{IF}(\omega_{IF}t)\right]^5\right\}$$

$$+ \ldots$$

$$= [a_1 2V_{IF} + \tfrac{3}{2}a_3 V_{IF}^3 + 3a_3 V_{IF}V_{LO}^2 + \tfrac{15}{4}a_5 V_{IF}V_{LO}^4 + \tfrac{15}{2}a_5 V_{IF}^3 V_{LO}^2 + \tfrac{5}{4}a_5 V_{IF}^5]\cos(\omega_{IF}t)$$

$$+ [\tfrac{1}{2}a_3 V_{IF}^3 + \tfrac{5}{3}a_5 V_{LO}^2 V_{IF}^2 + \tfrac{5}{8}a_5 V_{IF}^5]\cos(3\omega_{IF}t)$$

$$+ [\tfrac{2}{3}a_3 V_{IF}V_{LO}^2 + \tfrac{5}{2}a_5 V_{IF}V_{LO}^4 + 5a_5 V_{IF}^3 V_{LO}^2]\cos[(2\omega_{LO} + \omega_{IF})t] \qquad \Rightarrow \textbf{ RF Signal}$$

$$+ [\tfrac{2}{3}a_3 V_{IF}V_{LO}^2 + \tfrac{5}{2}a_5 V_{IF}V_{LO}^4 + 5a_5 V_{IF}^3 V_{LO}^2]\cos[(2\omega_{LO} - \omega_{IF})t] \qquad \Rightarrow \textbf{ Image Signal}$$

$$+\tfrac{5}{8} a_5 V_{IF} V_{LO}^4 \cos[(4\omega_{LO} + \omega_{IF})t]$$

$$+\tfrac{5}{8} a_5 V_{IF} V_{LO}^4 \cos[(4\omega_{LO} - \omega_{IF})t]$$

$$+... \qquad\qquad\qquad\qquad\qquad\qquad\qquad (3.7)$$

From the above equations if the mixing frequency is expressed by $mf_{IF} + nf_{LO}$, we can conclude the features of the balanced subharmonic mixers in which the two diode pairs are excited by the out-of-phase LO and in-phase RF signals:

> kth-order responses arise only from the terms of the kth power in (3.3).

> All even-order spurious responses are eliminated.

> All (m, n) spurious responses are eliminated if m is even and n is odd, but not if m is odd and n is even.

3.3. Substrate Material and Diodes

3.3.1. Substrate Material

It is very important to select a proper substrate material before we start our design. We have to consider both electrical and mechanical properties. The high dielectric constant can reduce the size of the circuit. But it also causes more loss in the designed circuit. The Alumina ceramic substrate has higher fabrication precision than usual soft substrates, but the substrate has less flexibility and it is easier to be broken than the soft substrates. *We have wasted several months time just because of the mechanical difficulty in an Alumina ceramic substrate.*

In this design, Rogers RT/Duroid® 6010LM was finally chosen as the substrate material. It has following characteristics:

1) High dielectric constant, leading to smaller circuit size.

2) Low loss, which is deal for operating at Ku-band or below.

3) Low moisture absorption that reduces effects of moisture on electrical loss.

4) Tight ε_r and thickness control for repeatable circuit performance.

5) Soft and flexibility, easy to be cut in an arbitrary shape.

Rogers RT/duroid® 6010LM Substrate Specifications considered in the design are:

- Dielectric constant: $\varepsilon_r = 10.2$

- Substrate thickness: $h = 10$ mil

- Metalization thickness: $t = 0.7$ mil

- Loss tangent: $\tan \delta = 0.0023$

3.3.2. Diodes

ALPHA DMK2308-000 GaAs Schottky-barrier anti-parallel diodes are selected as the mixing devices because of its high performance and competitive market prices. The single junction's parameters of ALPHA DMK2308-000 are show in Table 3.1.

Table 3.1 Single junction's parameters of ALPHA DMK2308-000

Spice Parameters (Per Junction)

I_s Amp	R_s Ω	n	T_D S	C_j0 pF	m	E_G eV	V_J eV	X_{TI}	FC	B_v V	I_{BV} A
0.5 E-12	4	1.05	1E-11	0.05	0.26	1.43	0.82	2	0.5	4.0	1E-05

ALPHA GaAs Schottky-barrier diodes have lower junction capacitance and low series resistance (two important parasitics), as well as a better I/V characteristic. Anti-parallel diodes offer symmetrical I/V curve. From the previous analysis in section 3.2, the identical diodes characteristics are very important for a balanced subharmonic mixer to achieve the low conversion loss, low noise and inherent rejection of $2f_{LO}$ and all other spurious responses.

ALPHA GaAs Schottky-barrier diodes are designed for MIC work (hard and soft substrates), but the leadless design eliminates the problems associated with mounting of beam lead diode. Due to its rigid construction, it exceeds environmental requirements for MIC and hybrid applications. The standard packaging is in a gel pack and its outline dimensions are shown in Figure 3.3.

Anti-Parallel - DMK2308-000
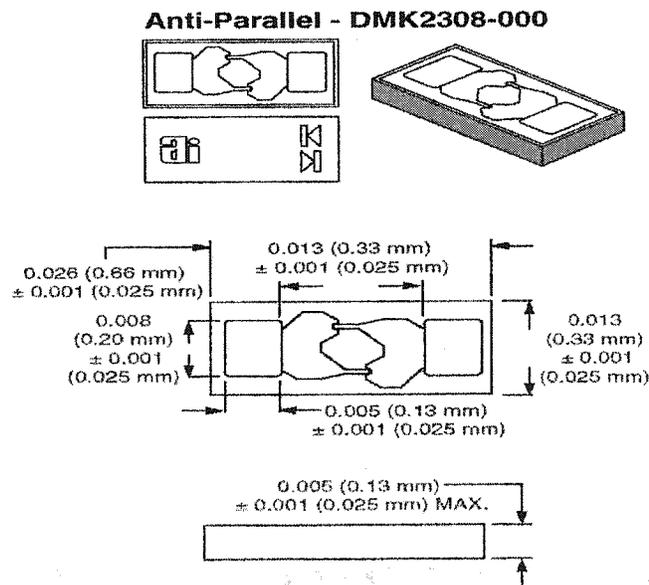
Figure 3.3 ALPHA DMK2308-000 packaging outline dimensions.

3.4. Structures and Design of Balanced Subharmonic Upconverter

The proposed balanced subharmonic upconverter is shown in Figure 3.4. It mainly consists of five parts, namely, a band-pass filter, a low-pass filter, a matching network, two anti-parallel diode pairs (ALPHA DMK2308-000 used in our design) and an 180° ring hybrid. All of the parts are realized on the same substrate board (Rogers RT/duroid® 6010LM).
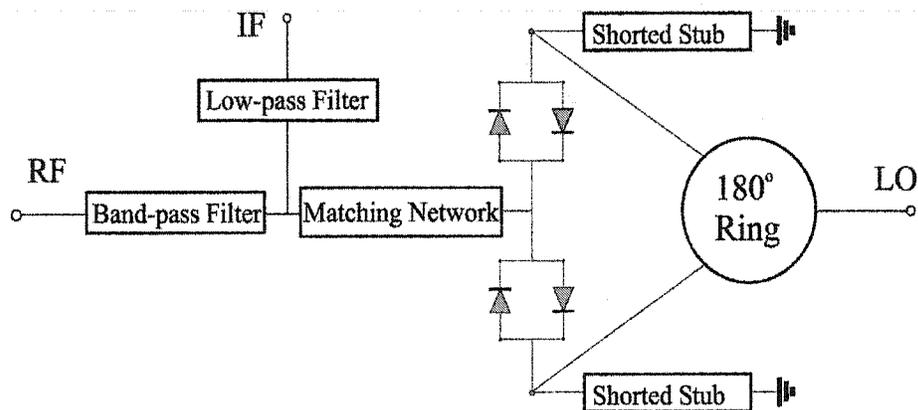
Figure 3.4 Balanced subharmonic mixer schematic

The band-pass filter is connected to the RF port for RF signal extraction. It is a four-stage coupled-line filter, which is designed to pass the RF ($2f_{LO}+f_{IF}$) signal (around 15 GHz), and provide an open circuit to IF signal (around 1 GHz), rejecting the image ($2f_{LO}-f_{IF}$) signal (around 13 GHz) and other unwanted mixing products. The band-pass has been well designed.

The low-pass filter with maximum flat characteristic consists of three open stubs and it is connected to the IF port. This is designed to pass the IF signal (around 1 GHz) and to

prevent the RF $(2f_{LO}+f_{IF})$, LO (7 GHz) and image $(2f_{LO}-f_{IF})$ as well as to reject some unwanted mixing products at the IF port. This low-pass filter has been well made and presented in the previous chapter.

The two anti-parallel diode pairs are the mixing devices. As the mixing devices, they must have a strong non-linearity, low noise, low distortion, and adequate frequency response. In this design, the ALPHA DMK2308-000 GaAs Schottky-barrier anti-parallel diodes are selected as the mixing devices.

The 180° ring hybrid is used to supply an equal magnitude and opposite phase of the LO signal for the two diode pairs. The equal magnitude permits the both diode-pairs to work at the optimum condition. As we have already proved theoretically at section 3.2, feeding the opposite phase LO can eliminate some spurious signals. The two $\lambda_{g,\,RF/2}$ (or $\lambda_{g,\,LO/4}$) shorted stubs are located at the LO side of the anti-parallel diode pairs such that the diodes are terminated with a short circuit at RF frequency, but the LO signal is less affected because the LO frequency is set to be half of the RF frequency. The use of the two shorted stubs also provide DC/IF return paths to ground. Through the ring with two additional $\lambda_{g,\,LO/2}$ length series lines towards the two diode pairs, the LO signal is split equally and applied by the phase difference of 180°. Therefore, the point of interconnection between the two diode pairs is a virtual ground at the LO frequency for the LO excitation.
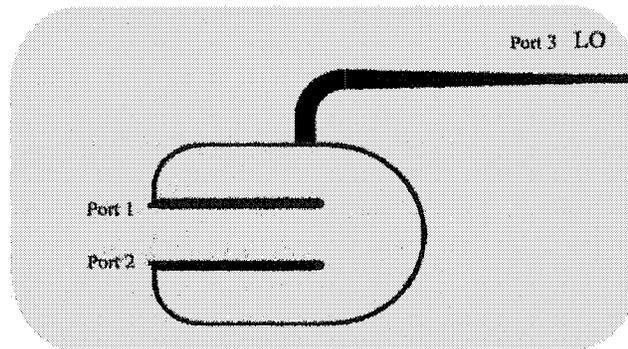
Figure 3.5 Layout of 180° ring hybrid.

Figure 3.5 shows the layout of the 180° ring hybrid. It is a three-ports circuit in which the port 3 is connected to the LO source, port 1 and port 2 are to the two anti-parallel diode pairs, respectively. The 180° ring hybrid consists of two shorted stubs with two additional $\lambda_{g,\,LO/2}$ length series lines and a tapered T-junction.

The 180° out-of-phase ring hybrid circuit is simulated and optimized with the aid of HP ADS. Figure 3.6 shows the EM simulation results for the final designed ring.

The internal impedance of the anti-parallel Schottky-barrier diode pairs are vary with the operating frequency and power level of LO source. It is also very sensitive to the loading condition of the non-linear devices at various idler frequencies. The mixing diodes should have a resistive load at LO, RF and IF frequencies, and a reactive loads at all other mixing frequencies generated in the non-linear device to avoid any power loss, which increases the conversion loss of the mixer. However, the mixer performance strongly depends on the nature of the reactive load (short, open, capacitive or inductive).
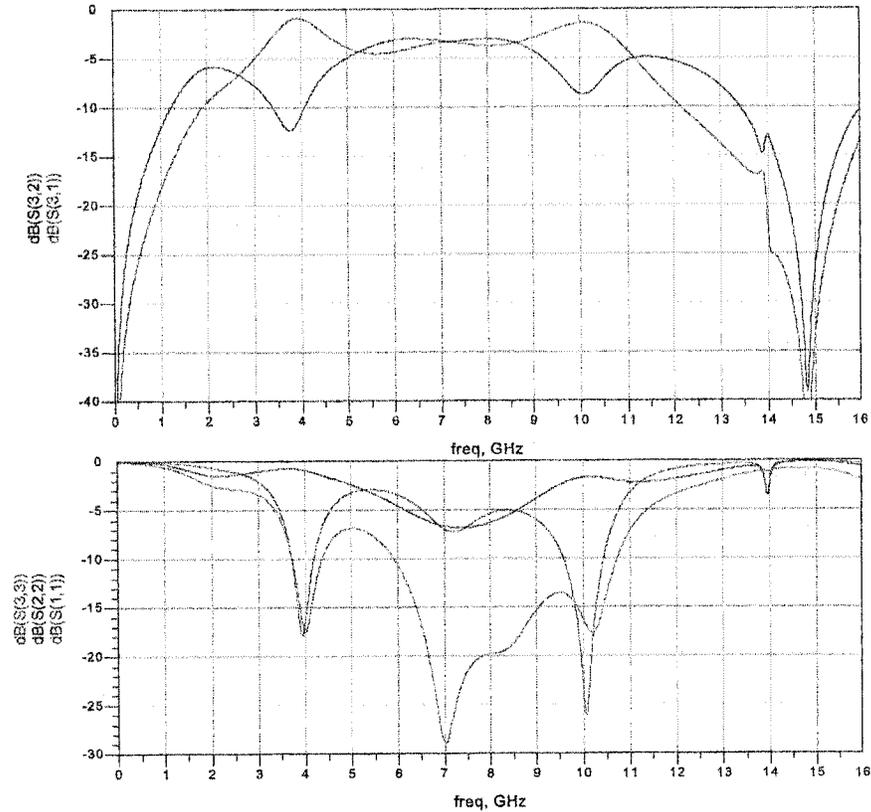
Figure 3.6 180° out-of-phase ring simulation results.

We can estimate optimum loads at idler frequencies from actual measurement or derive it from the ideal generic circuit model with the generic algorithm[4]. The matching network is designed to allow the optimum impedance matching at RF frequency for low conversion loss and wide input/output dynamic range. Normally, it is difficult to realize such an upconverter having wide input/output dynamic range, minimum conversion loss, highest RF power output and lowest LO pumping. Therefore, we perform some tradeoff

among them during the optimization of the matching network in the balanced subharmonic upconverter.

3.5. Performance

3.5.1. Simulation Results

Figure 3.7 shows the balanced subharmonic upconverter schematic in ADS based on EM models for three blocks: a band-pass filter, a ring hybrid circuit and a matching network with IF low-pass filter. EM-simulated S parameters describe properties of the three block models in a more accurate manner. The diode pairs are created by a non-linear PN junction diode model available in the HP-ADS component library.
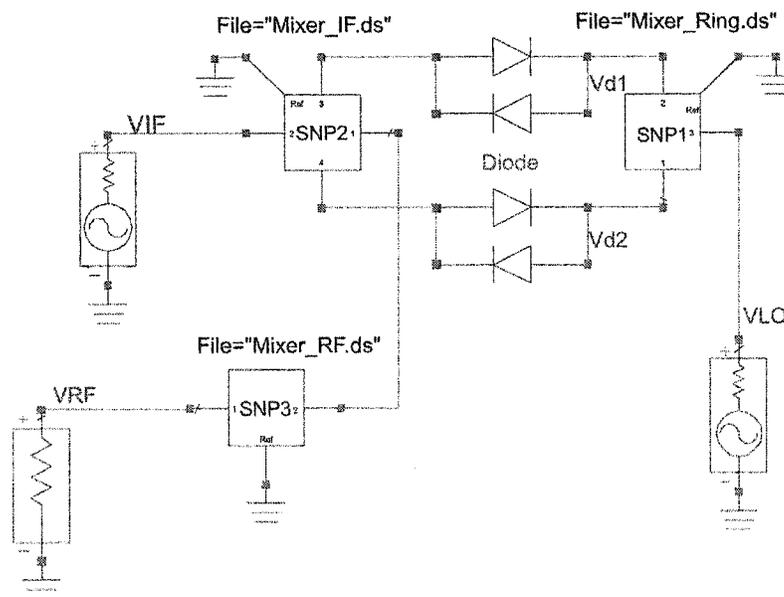
Figure 3.7. Balanced subharmonic upconverter schematic in ADS
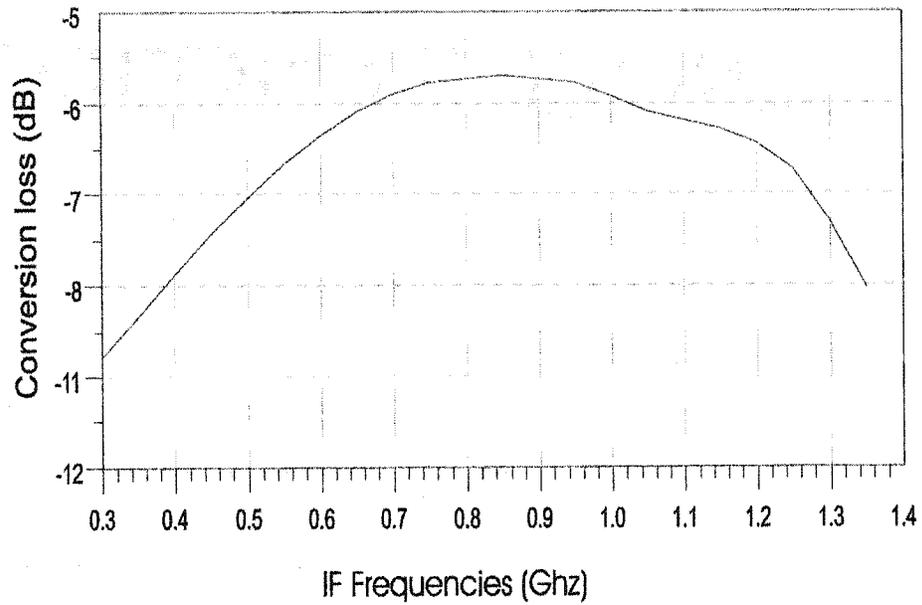
Figure 3.8 Simulated conversion loss vs. IF frequencies.
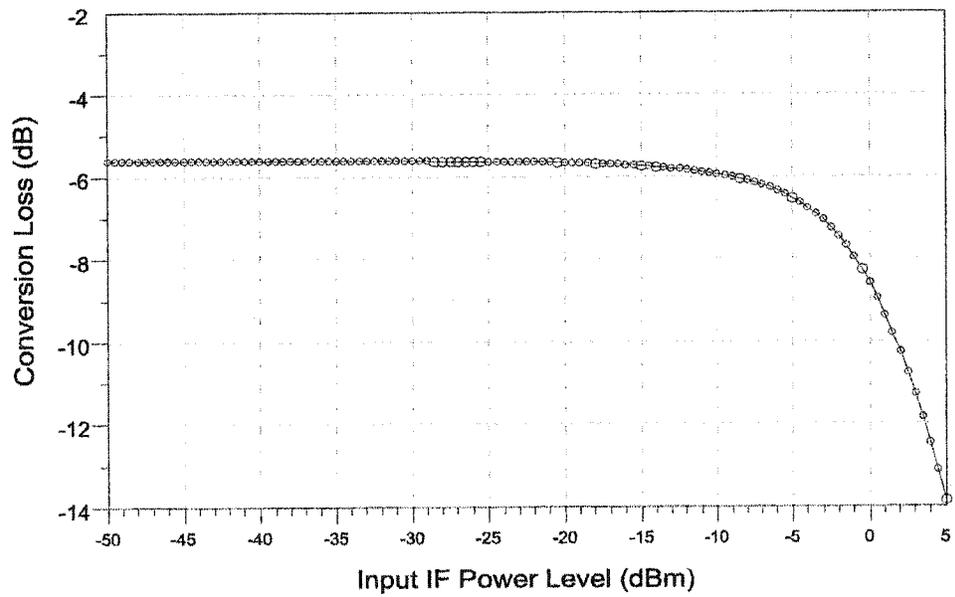
Figure 3.9 Simulated conversion loss vs. IF power.

Figure 3.8 shows the simulated conversion loss versus IF frequency at a fixed LO of 7 GHz frequency and 6.0 dBm power level, where the IF input power level is –20 dBm. From Figure 3.8, it can be seen that the conversion loss varies with frequency. The lowest conversion loss point is around –5.7dB at the IF frequency of 800 MHz.

Figure 3.9 shows the simulated results of mixer conversion loss versus the input IF power. We set IF frequency at 1 GHz and LO frequency at 7 GHz with power level 6.0 dBm, then we sweep the input IF power level from –50 dBm to 5 dBm. It can be seen that the simulated conversion loss is about 6.0 dB over a large dynamic range of –50 dBm to -6 dBm. The 1-dB compression point is around –4.2 dBm.

Figure 3.10 shows the simulated spectrum at the output of RF in the balanced subharmonic mixer when the LO power is 7 GHz with 6 dBm power injected at the LO port and the IF signal is 1 GHz with –17 dBm power applied at the IF port. From the simulated spectrum, it can be seen that there are only four spectral components observed obviously. The mark 1 stands for the RF frequency of 15 ($2f_{LO}+f_{IF}$) GHz at –25.228 dBm. The mark 2 is for the image response that is 13 ($2f_{LO}-f_{IF}$) GHz with –41.772 dBm, 16.5dBc suppression below the RF signal. The mark 3 is for the third-order LO harmonic of 21 GHz with –41.587 dBm, and it is 47.587dBc below the LO signal. The mark 4 is for the fourth-order LO harmonic of 29 ($4f_{LO}+f_{IF}$) GHz, which has much lower power level of –52.01 dBm. In addition, the second-order LO harmonic of 14 GHz and all even order (2,2) spurious response cannot be seen. Those results are identical with the previous analysis presented above.
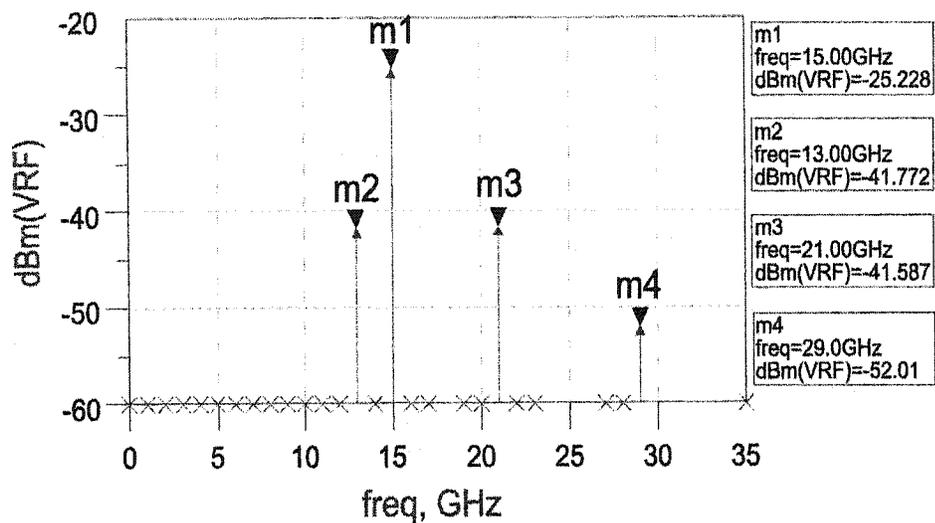
Figure 3.10. Simulated spectrum at the RF output in the balanced subharmonic upconverter

3.5.2. Measurement Results

The photo of the fabricated balanced subharmonic upconverter is shown in Figure 3.11.
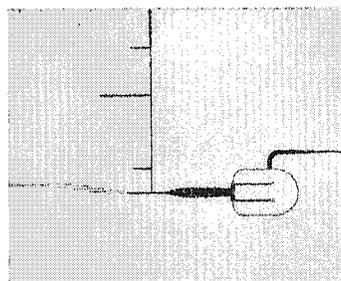

Figure 3.1. The photo of the fabricated balanced subharmonic upconverter

There are several measurement instruments used in the upconverter performance test. Two signal generators, HP 83721B and ROHDE & SCHWARZ SMR40, are used as IF signal and LO power source, respectively. The spectrum analyzer, ROHDE & SCHWARZ FSIQ40, is used for the measurement of power spectral distribution at the output of RF in the balanced subharmonic upconverter. A power meter, ANRITSU ML2438A, is used for the purpose of actual power measurement. The balanced subharmonic upconverter is mounted on a three-port universal test fixture (ANRITSU 3086). The cable losses at RF, IF and LO frequencies are determined using a calibration approach and are de-embedded from the measured data. The other additional losses of coaxial-to-microstrip transitions are not taken into account.
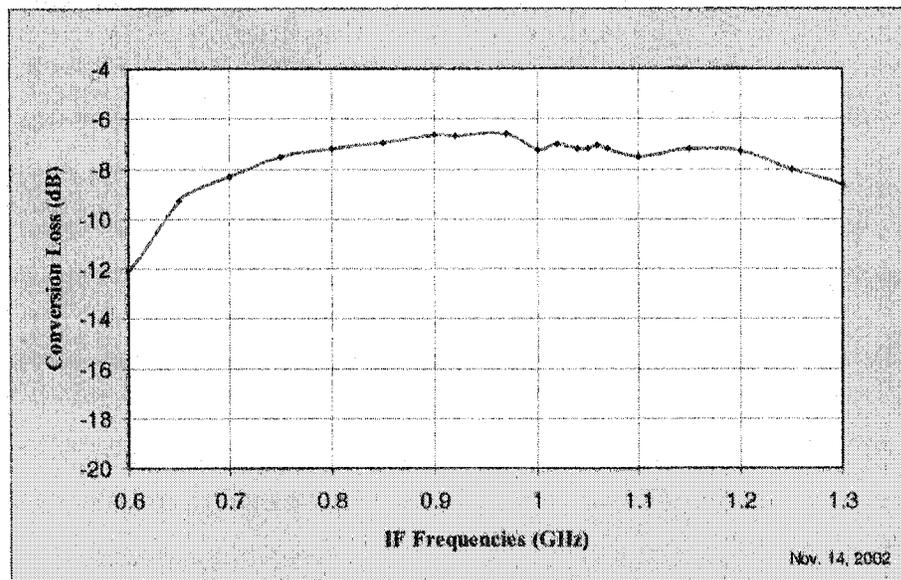
Figure 3.12. Measured conversion loss vs. IF frequencies

Figure 3.12 shows the measured conversion loss versus IF frequencies when the IF is swept from 600 to 1300 MHz with a constant input power level of –20dBm and the LO is

fixed at the frequency of 6.75 GHz with 8.5 dBm power level. The measured conversion loss is less than 8 dB over the IF frequency range of 720-1250 MHz. The lowest conversion loss is measured at 900 MHz and is equal to 6.6 dB. The measured conversion loss is very close to the simulated result.
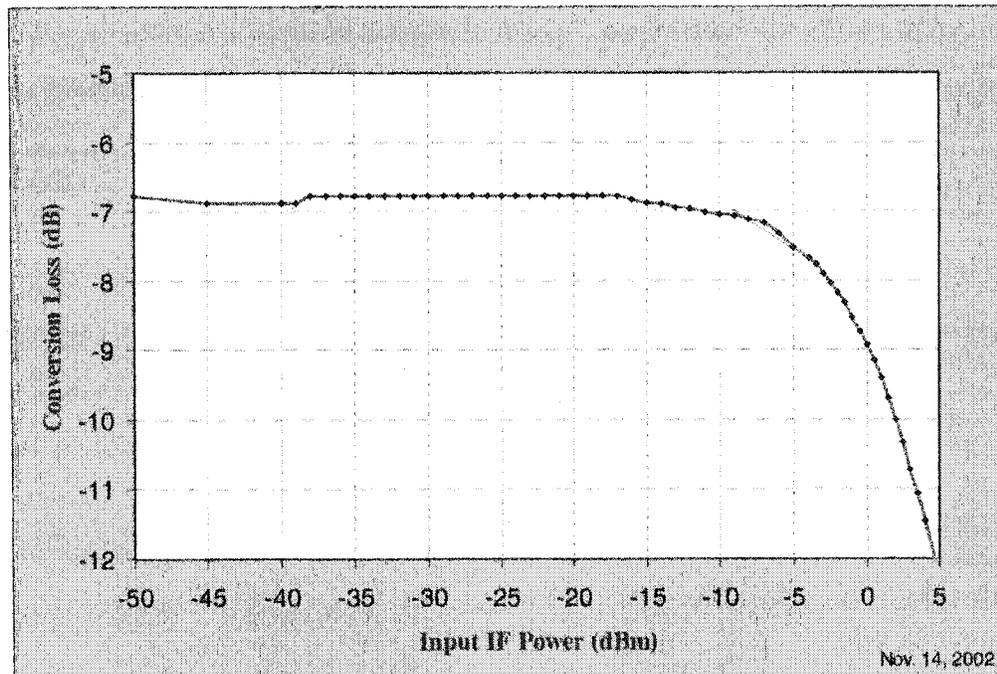

Figure 3.13. Measured conversion loss vs. input IF power level

Figure 3.13 shows the measured conversion loss versus input IF power level, where IF frequency is set at 0.9 GHz and LO frequency at 6.75 GHz with 8.5 dBm power level; input IF power level is swept from −50 dBm to 5 dBm. The measured conversion loss is around 6.8 dB over a large dynamic range. Below the IF power level of −10 dBm, the conversion loss is almost constant. Beyond the IF power of −6 dBm, the conversion loss drops quickly. The reason is that the diodes are driven into their saturation region. From

this Figure, it can also be seen that the input 1-dB compression point is around −4 dBm. A very good agreement is achieved between measurement and simulation.
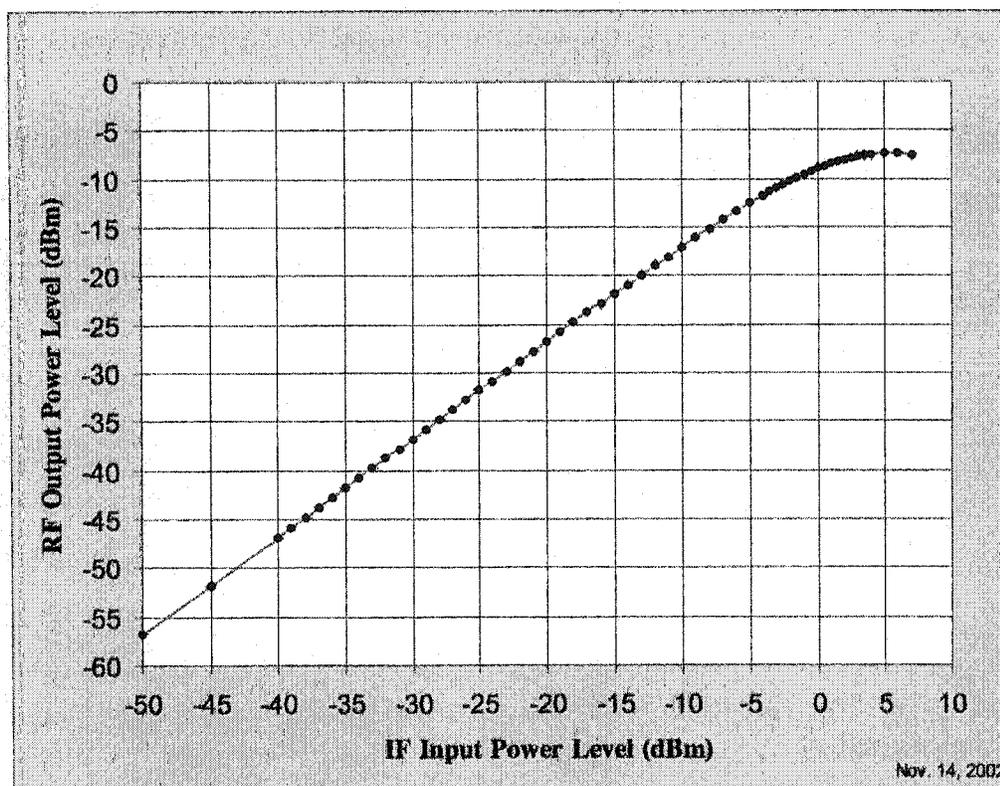

Figure 3.14. Measured RF output vs. IF input power level.

Looking at the measured RF output versus IF input power as shown in Figure 3.14, we can observe that a good linearity and a wide input/output dynamic range are achieved with our upconverter design.

3.6. Conclusion

We have discussed the inherent properties of balanced subharmonic mixer. Through our analysis based on the ideal cases, the basic conditions for the realization of such an upconverter has been confirmed, namely, the LO signal with 180° out-of-phase and the IF signal with in-phase at two anti-parallel diodes.

To be more flexible for the further development of spatial waveguide array upconverter, Rogers RT/duroid® 6010LM substrate has been selected for the realization of a Ku-band balanced subharmonic upconverter.

Based on our designed low-pass and band-pass filters, a matching network has been optimized for low conversion loss and wide input/output dynamic range. Physical realization of the upconverter has demonstrated a good performance that features low conversion, high suppression capability of even-order harmonics and some spurious signals and good agreement between measured and simulated results.

CHAPTER IV

SPATIAL WAVEGUIDE ARRAY UPCONVERTER

4. SPATIAL WAVEGUIDE ARRAY UPCONVERTER

4.1. Introduction

It is known that the combining efficiency in the spatial combining architecture is constant with the number of elements combined, up to the physical limitation of the architecture. Spatial combining oscillator and amplifier were reported [5, 6, 7]. In those design, the spatial combined power sources are implemented as arrays of oscillators or amplifiers.

Spatial combined arrays of other components, such as phase shifters, mixers, and frequency multipliers, show the great potential for millimeter-wave applications. So far, no waveguide array mixers have been reported. With the well-justified design technique, we propose a new architecture of spatial power combining upconverter, which is developed at Ku-band for the proof of concept.

As we know, the operating linear range of mixer is normally limited at low input power so that its mixing output power is certainly obtained at a small power level. In the spatial power combining upconverter, the numbers of mixer circuits are spatially combined in a waveguide to be an array that couples the mixer circuits in free space. As such, the proposed architecture reduces the limitation of the mixer linear range at IF input port and increases the output power level at RF port.

The mixer in a microstrip format is a key building block in the spatial power combining upconverter. As we described in Chapter 3, the subharmonically pumped (SH) mixer is very useful at higher frequencies since it has the advantages of subharmonic

pumping and inherent suppression of local oscillator (LO) noise, both alleviating the demand for the LO source. On the other hand, the balanced mixer is also widely used due to its rejection of certain spurious responses, its reduction of LO noise and spurious signals as well as its enhancement of inherent LO-to-RF isolation. Therefore, a balanced harmonic mixer should be able to combine the advantages of both SH and balanced mixers if the mixer design is made in an adequate manner: 180° out-of-phase LO and in-phase IF (or RF). As a result, our proposed architecture is in the form of a spatial waveguide array, in which there are four unit cards of the microstrip balanced subharmonic upconverter loaded in waveguides. Since the LO frequency is almost ½ RF frequency, two different waveguides are used for LO and RF paths. That especially leads to an excellent isolation between RF and LO ports.

4.2. Transitions

There are microstrip-to-slotline and finline-to-waveguide transitions needed in the spatial waveguide array balanced subharmonic upconverter for spatial feed purpose on each unit board. The microstrip-to-slotline and finline-to-waveguide transitions are individually designed at LO and RF frequencies for both LO and RF paths. On the other hand, a waveguide-to-coaxial transition needs to be created at LO port for the purpose of measurement.

4.2.1. Microstrip-to-slotline transition

Microstrip-to-slotline transitions are widely used in microwave hybrid integrated circuit. There are several ways to construct a microstrip-to-slotline transition [8,9]. The typical and commonly used configuration is shown in Figure 4.1.
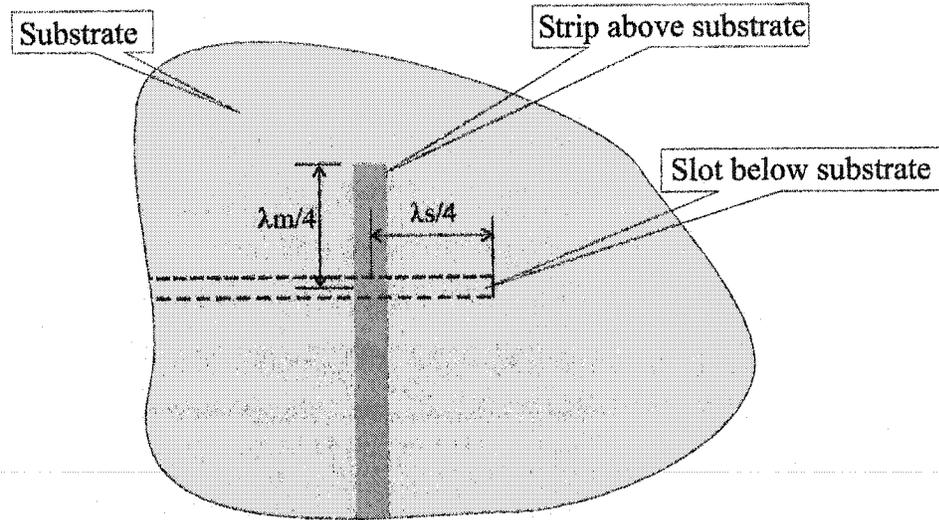
Figure 4.1. The typical microstrip-to-slotline transition

The typical microstrip-to-slotline transition is a two-level circuit. The slotline consists of a narrow gap in a conductive coating, which is etched on one side of the substrate, is crossed perpendicularly by a microstrip conductor on the opposite side. Both microstrip and slot extends about one quarter of a strip wavelength beyond the crossing point of the slotline and microstrip. Coupling between the slotline and the microstrip line occurs by means of the magnetic field [8, 9].

The equivalent circuit of a typical microstrip-to-slotline transition is shown in Figure 4.2 (a) [10]. The reactance X_{0s} represents the inductance of a shorted slotline, and C_{oc} is the capacitance of an open microstrip. Z_{os} and Z_{om} are slotline and microstrip characteristic impedances, respectively. θ_s and θ_m represent the electrical lengths (quarter-wave at center frequency) of the extended portions of the slotline and the microstrip line. The n is the transform ratio [11].
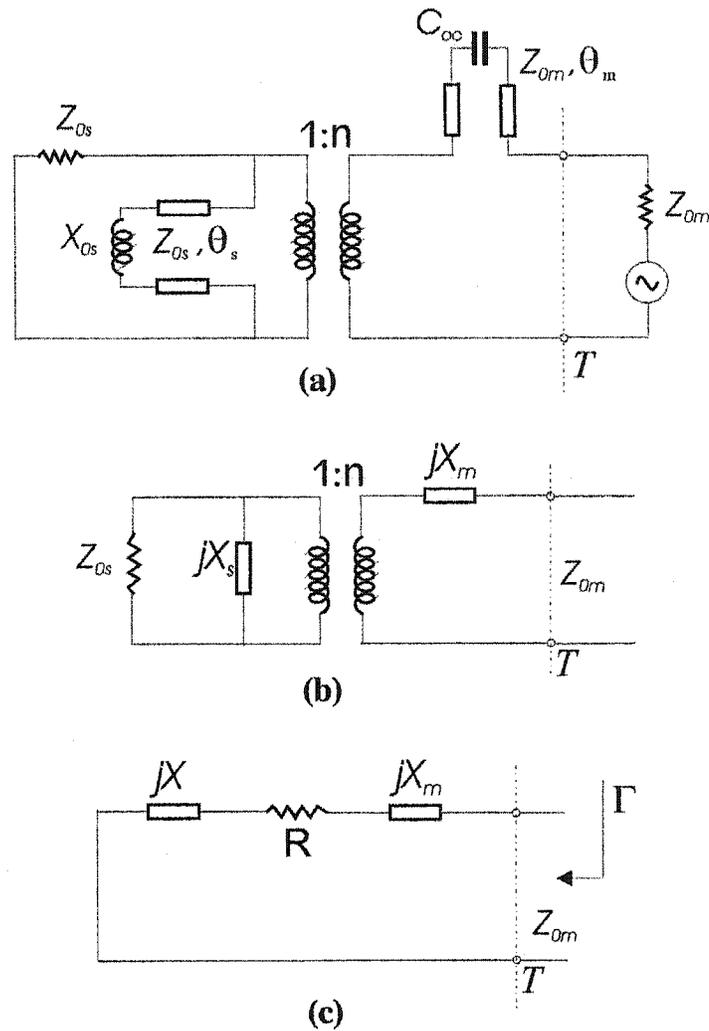
Figure 4.2 Equivalent circuit of a typical microstrip-to-slotline transition.

For the further analysis the equivalent circuit in Figure 4.2 (a) may be redrawn as in Figure 4.2 (b). Where,

$$jX_s = Z_{0s} \frac{jX_{0s} + jZ_{0s} \tan \theta_s}{Z_{0s} - X_{0s} \tan \theta_s} \tag{4.1}$$

and

$$jX_m = Z_{0m} \frac{1/j\omega C_{oc} + jZ_{0m}\tan\theta_m}{Z_{0m} + \tan\theta_m/\omega C_{oc}} \tag{4.2}$$

After transformation to the microstrip side, the equivalent circuit of Figure 4.2 (b) reduces to that is shown in Figure 4.2 (c). In this circuit,

$$R = n^2 \frac{Z_{0s}X_s^2}{Z_{0s}^2 + X_s^2} \tag{4.3}$$

and

$$X = n^2 \frac{Z_{0s}^2 X_s}{Z_{0s}^2 + X_s^2} \tag{4.4}$$

Finally, the input reflection coefficient Γ is given by

$$\Gamma = \frac{R - Z_{0m} + j(X_m + X)}{R + Z_{0m} + j(X_m + X)} \tag{4.5}$$

From the above analysis, we see that the reflection coefficient Γ depends on the transformer ratio n, the characteristic impedance of slotline Z_{0s} and the characteristic

impedance of microstrip line Z_{om}. The transformer ratio n is a function of frequency [11, 12].

Bandwidth limitation of the cross-junction transition results mainly from the frequency dependence of X and X_m (see Figure 4.2(c)). These reactances in turn depend on the stub length and ratio n. A short-circuited microstrip will minimize X_m, and an open-circuited slotline will minimize X. Alternatively, stub reactance can be so designed that there is a mutual cancellation of X and X_m and $R = Z_{0m}$.

If the substrate is selected as the one we used for the design of the microstrip balanced subharmonic upconverter (Rogers RT/duroide® 6010LM), the minimum slotline characteristic impedance Z_{0s} can be fabricated around 90Ω and the maximum microstrip line characteristic impedance Z_{0m} is 62Ω due to the fabrication tolerance in our lab. So, this situation may cause a limitation on tuning Z_{0s} and Z_{0m} to obtain a low return loss Γ for the design of the microstrip-to-slotline transition with a typical structure.

Even though adjusting the extended open stub electrical length θ_s and θ_m was attempted, it had certain effects on the transition bandwidth and insertion loss because there is no good matching between microstrip and slotline. Therefore, we have to modify the cross-junction configuration by setting a step on microstrip stub at the cross-junction of transition. This step acts as a reactance transform function. And it also makes a discontinuous jump at the cross-junction point, which can significantly reduce the transition return loss, without degrading the bandwidth. In such a way, there is on additional matching network to be needed.

There are two microstrip-to-slotline transitions designed at LO and RF paths, respectively. The optimum designed layout structures are shown in Figure 4.3. From our previous discussion, for a better return loss, we let the slot width Ws to be 5mil, and the width Wn of microstrip open stub is 4mil. Those are the minimum realizable values for fabrication in the lab.

Both RF and LO transitions have similar configurations. The only difference is at the open/short stub's lengths. The LO transition's open/short stubs are roughly twice longer than the RF, since the LO frequency is about half of RF frequencies. Figure 4.3(b) is the optimum designed layout structures for RF transition. The slot width Ws_0 is 5mil, and the width Wn_0 of microstrip open stub is 4mil. The slotline short stub lengths of Ls_0 for LO path and Ls for RF path are 153.5mil and 54.5 mil, respectively. The microstrip open stub lengths of Ln_0 for LO path and Ln for RF path are 149mil and 52.5 mil, respectively. The 50 Ω microstrip width Wm_0 are 8.7mil.
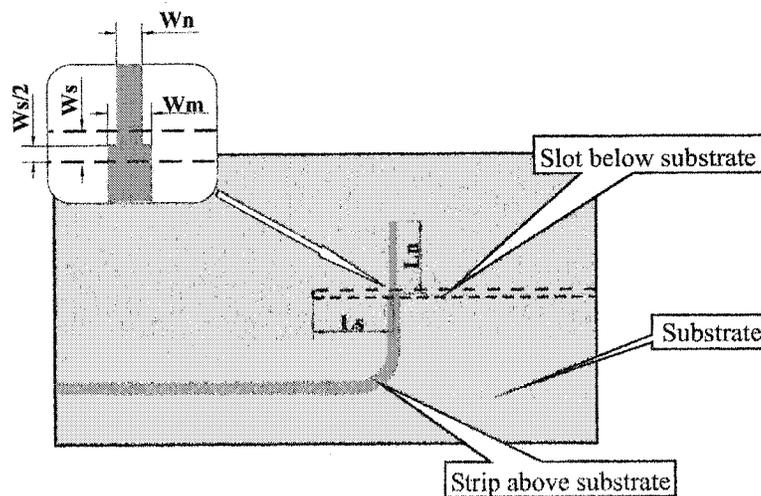
(a)
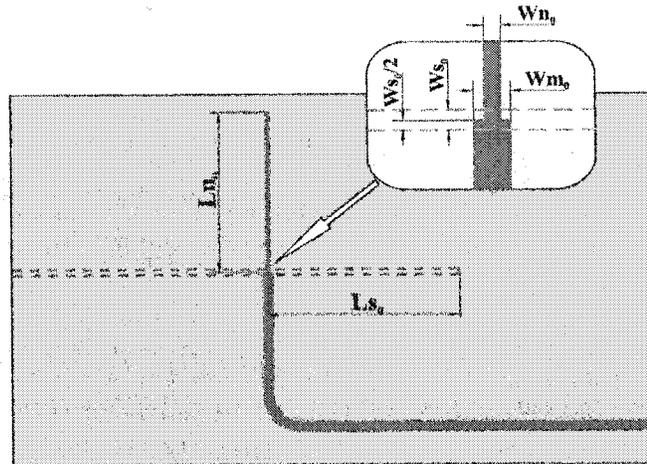
(b)

Figure 4.3. Structures of the microstrip-to-slotline transitions (a) RF transition. (b) LO transition.
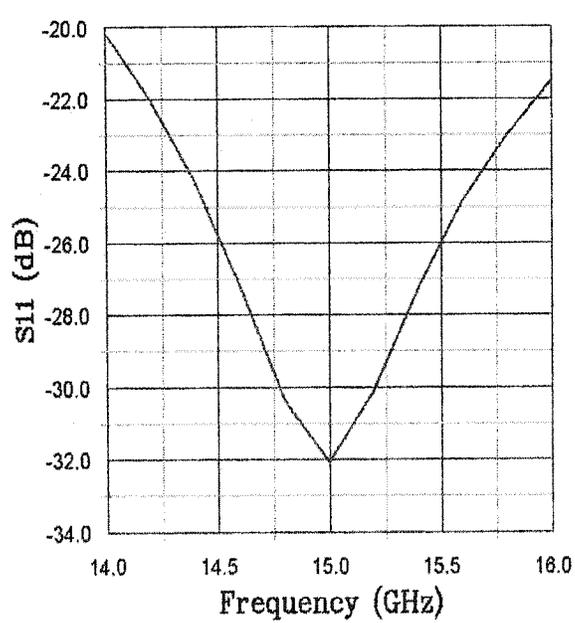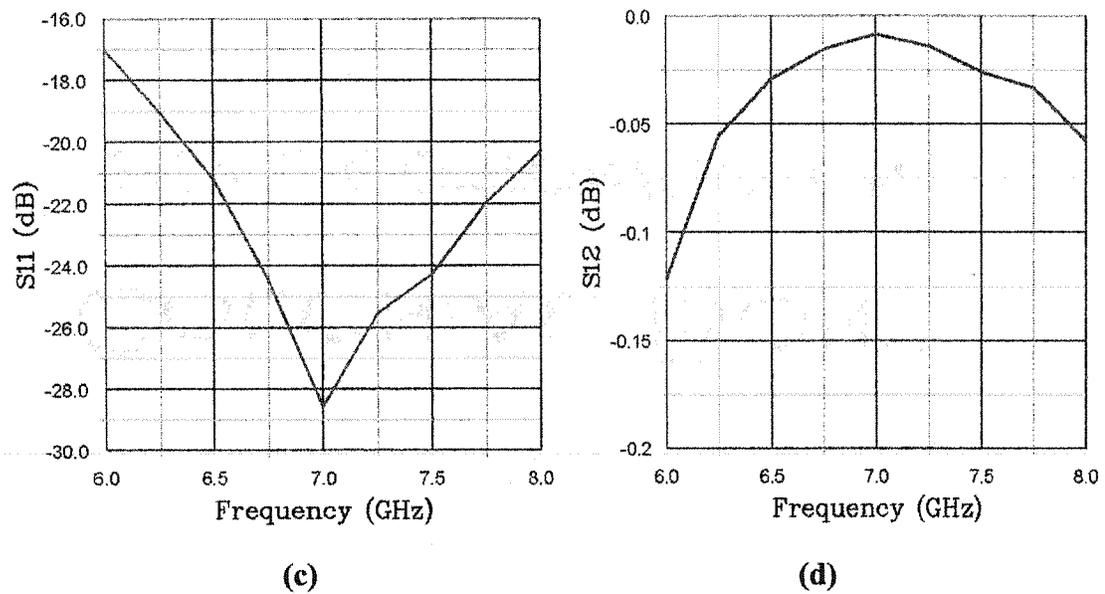

(a)
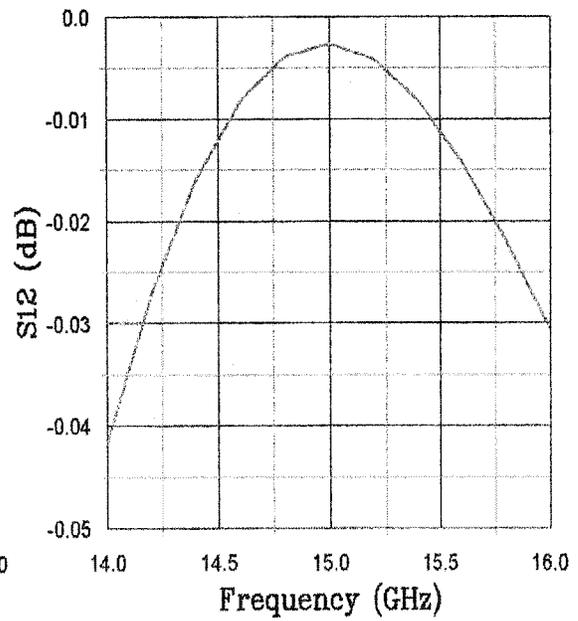
(b)

Figure 4.4. Simulated results of microstrip-to-slotline transitions.

An electromagnetic simulator Agilent HFSS (version 5.6) is used to simulate and optimize the transition structures. The simulation results are shown in Figure 4.4.

4.2.2. Finline-to-Waveguide Transition

Finline is a quasi-planar transmission line structure. The basic finline can be considered as a shielded slotline, with the slotline mounted in the E-plane of a rectangular waveguide.

There are two finline-to-waveguide transitions to be designed, which are used at both LO and RF sides for the LO power supply and RF signal output. Figure 4.5 shows the layout structures of those two transitions.
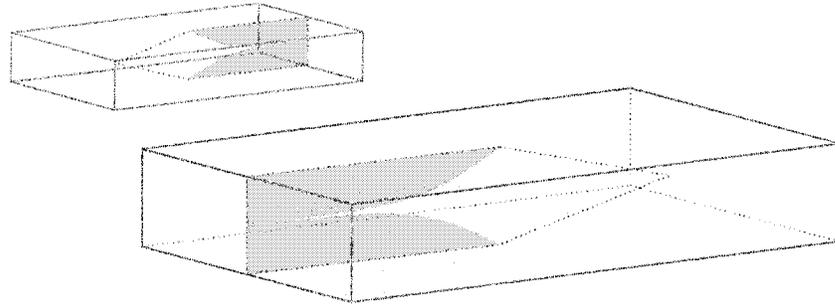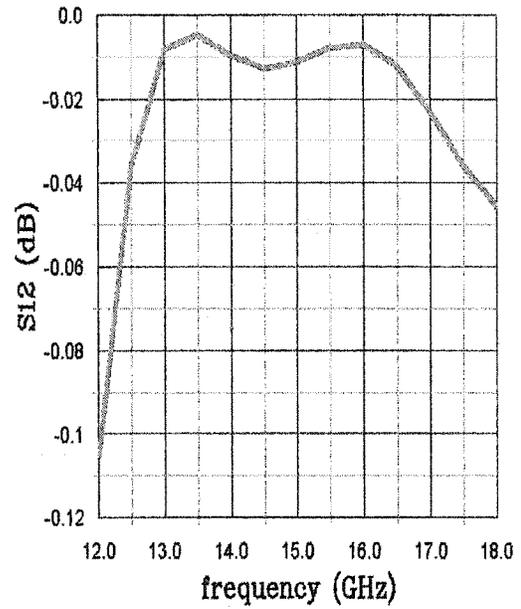

Figure 4.5 Structures of waveguide-to-finline transitions.

In Figure 4.5, a tapered finline is employed between the slotline and a rectangular waveguide where the slot width of the finline is gradually increased to the full height of the waveguide, which is used for smoothly transforming impedance and avoiding the reflection. To reduce the discontinuity between the finline with $W/b=1$ and the air-filled rectangular waveguide, a quarter-wave transformer in the form of a tapered protrusion. The finline dimensions determine the transition operating central frequency and its frequency bandwidth in the given waveguide. Agilent HFSS (version 5.6) is used to simulate and optimize the transition structures. The simulation results are shown in Figure 4.6.
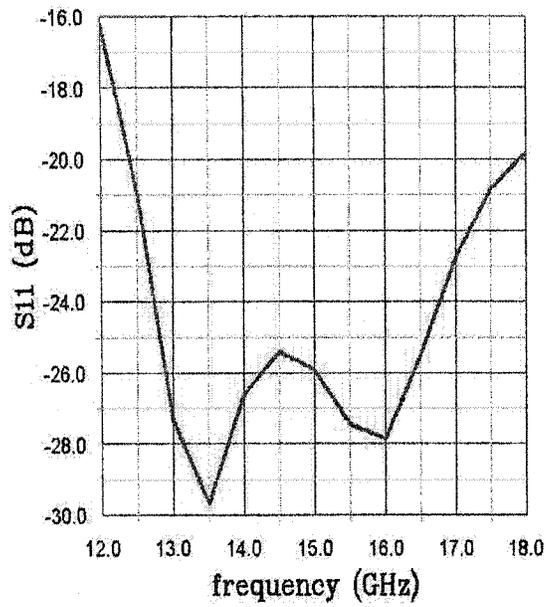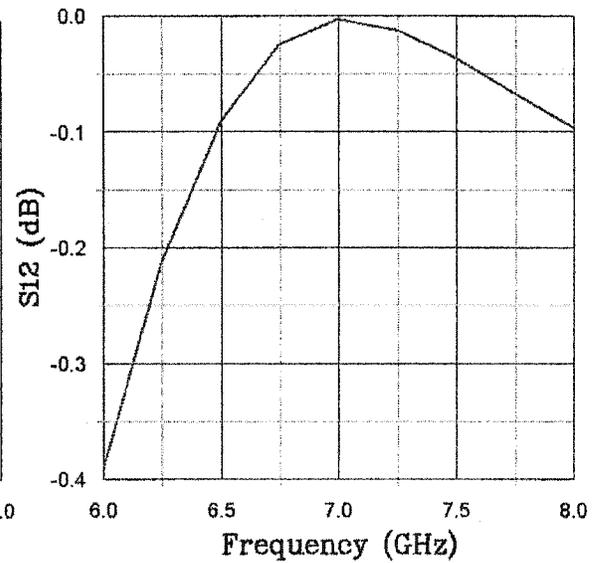
(a)

(b)
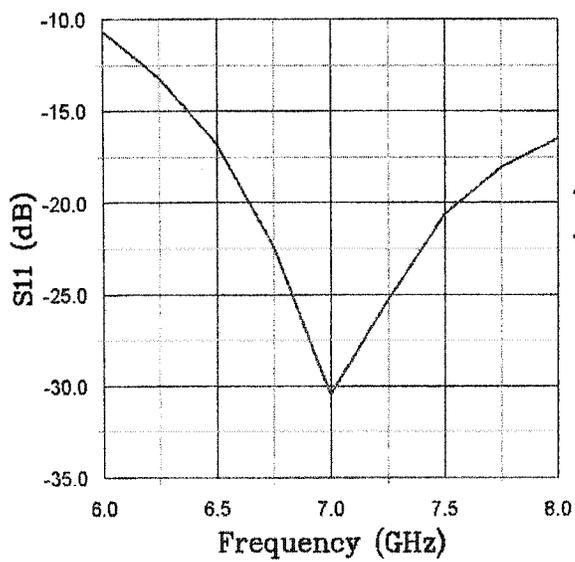
(c)

(d)

Figure 4.6. Simulated results of waveguide-to-finline transitions

4.2.3. Microstrip-to-Waveguide Transition

The whole microstrip-to-waveguide transition is the combination of the microstrip-to-slotline and finline-to-waveguide transitions with a certain space between the two transitions shown in Figure 4.7. If the space is not probably selected, the discontinuities for the two transitions in the whole structure might leads to a worse return loss in the case of a shorter space, or a high insertion loss in the case of a longer space.

To optimize the space between the microstrip-to-slotline and finline-to-waveguide transitions, the whole microstrip-to-waveguide transition is synthesized with the aid of a commercial full-wave simulator such as HFSS. The final simulation results are shown in Figure 4.8.
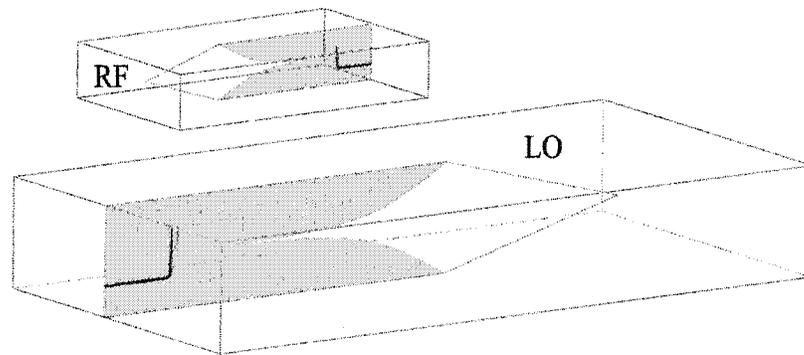
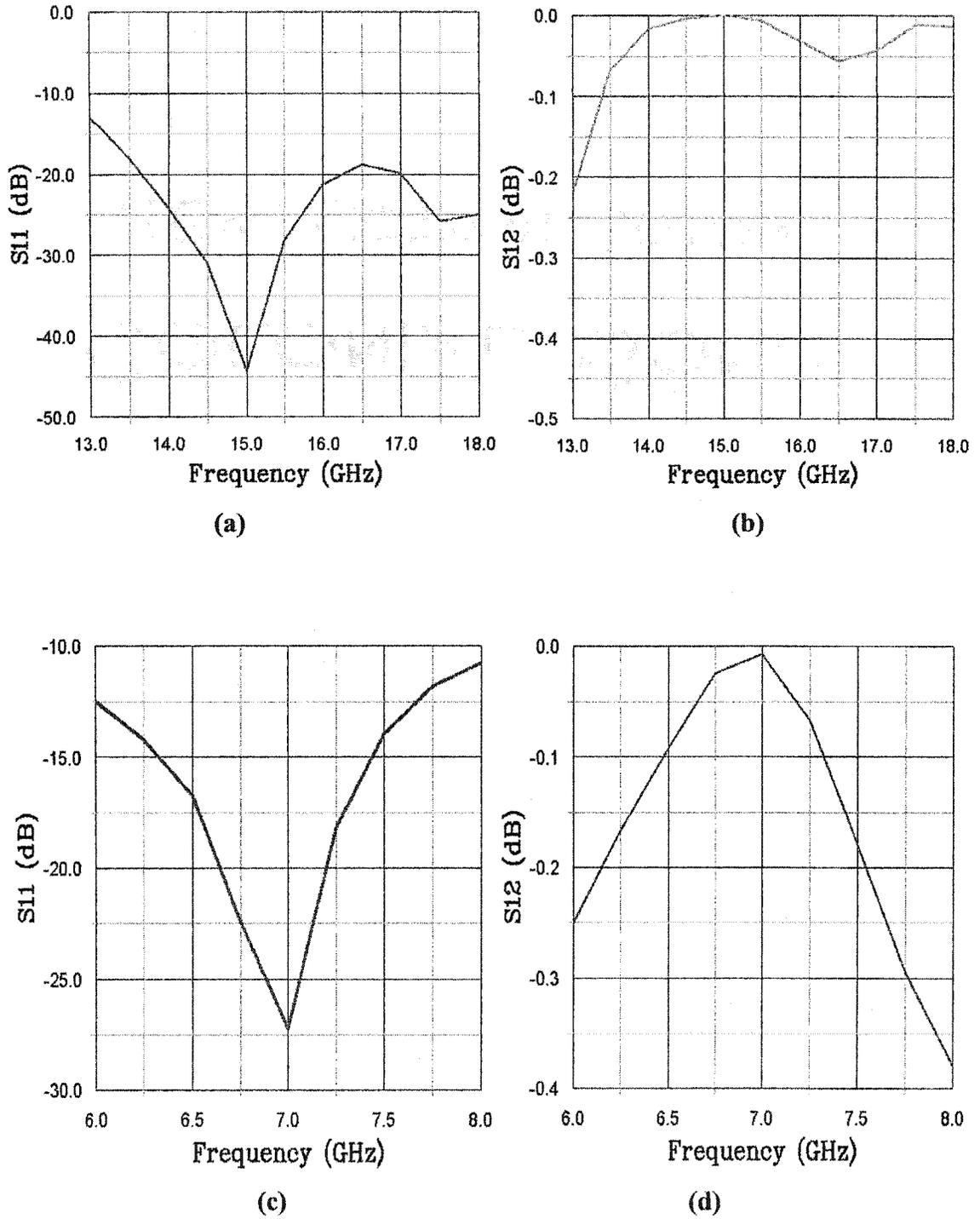Figure 4.7. Structure of whole microstrip-to-waveguide transitions

Figure 4.8. Simulated results of microstrip-to-waveguide transitions

4.2.4. Waveguide-to-Coaxial Transition

For the purpose of measurements, a waveguide-to-coaxial transition for LO power supply is designed. The structure of the waveguide-to-coaxial transition is shown in Figure 4.9. In this structure, the waveguide is a standard C-band rectangular waveguide (WR137) and the pin of a standard SMA connector is used as a probe in the waveguide.
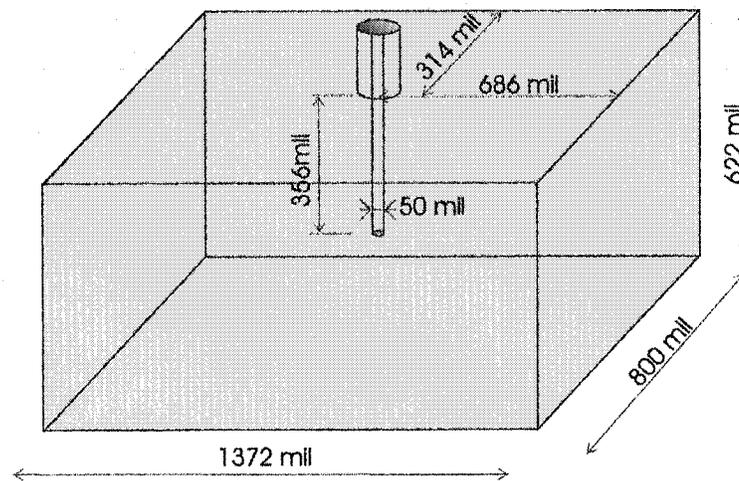

Figure 4.9. Structure of waveguide-to-coaxial transition

In general, the design theory requires that we place an electric probe at a point of the maximum electric field in the undisturbed guide, or place a magnetic loop to encircle the maximum number of magnetic field lines. So, the major portion of the design is the concern to find the best location, height, and diameter of the probe, to achieve optimum impedance match. The impedance of the TE_{10} mode in a rectangular waveguide is of the order of few hundred Ohms, whereas the coaxial line usually will have the much lower impedance, typically 50 Ω. This requires a high transformation ratio for the impedance match to the probe. There are some techniques to optimize the impedance match [13].

For a rectangular waveguide, the useful bandwidth usually starts at 25 percent [14] over the cut-off frequency of the TE_{10} mode and ends at the cut-off frequency of the TE_{20} (the next higher mode). A coaxial line supports a TEM mode, and which is very broadband as compared to the rectangular waveguide. Thus, a well-designed transition from coaxial line to waveguide transition will have, at best, the bandwidth of the waveguide.

Since it is a narrow bandwidth for LO path, we simply design the narrow-band waveguide-to-coaxial transition. A commercial full-wave simulator in Agilent HFSS (version 5.6) is used to simulate and optimize the transition. The simulation results are shown in Figure 4.10, where the diameter of probe is 50mil, the probe length is 356mil, and the distance between the probe and short-back wall is 356mil.
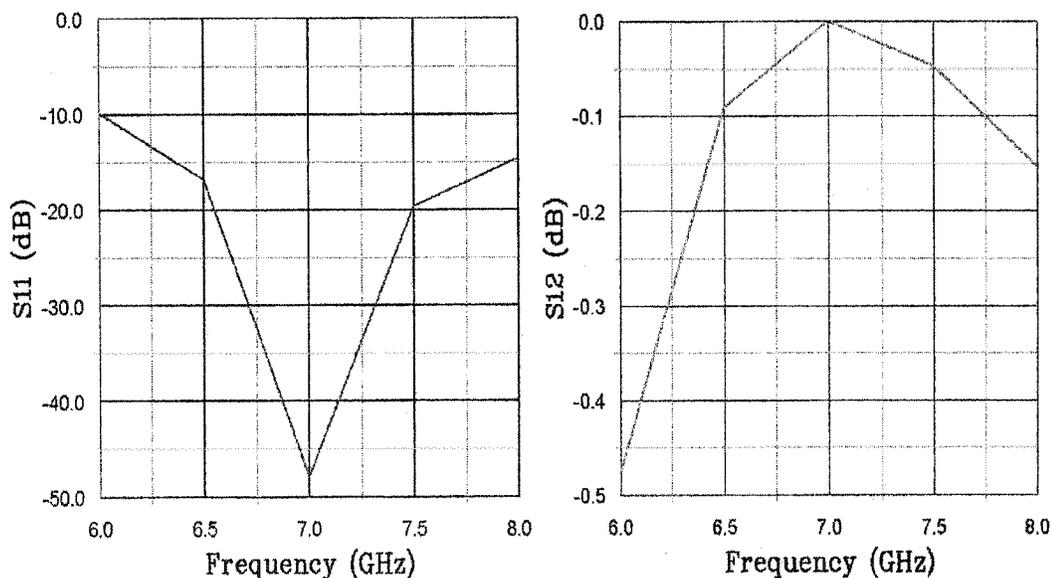
Figure 4.10. Simulated results of waveguide-coaxial transition

4.3. Spatial Waveguide Array Upconverter

The power is combined or divided spatially in the spatial waveguide array upconverter. In this case, the TE_{10} and TE_{20} modes can propagate at a particular operating frequency. By using a symmetric loading of structure, TE_{20} mode can effectively be suppressed [7]. So, our proposed architecture of spatial waveguide array upconverter is developed by inserting four balanced harmonic upconverter cards in the waveguide as an array. To easily verify our approach, the spatial waveguide array upconverter with single mixer unit card is firstly designed. Then, the approach is applied to the spatial waveguide array upconverter with four mixer unit cards.

4.3.1. Structure Description

The proposed structure of spatial waveguide array upconverter is shown in Figure 4.11. It is implemented as an array of four upconverter unit cards. Note that the number of cards can be increased. These unit cards are symmetrically loaded in the middle of the waveguide and are spaced equally by 90 mil from card to card. Each of the mixer unit cards consists of a balanced subharmonic upconverter in microstrip format, LO waveguide-to-microstrip transition and RF microstrip-to-waveguide transition. They are integrated on the same substrate (Rogers RT/duroid® 6010LM) of 10mil thickness.

Figure 4.12 shows the electric field lines of TE_{10} mode inside the rectangular waveguide. For the each of unit cards, it can makes one contribution to the electric field the end of 2-D upconverter card. The TE_{10} modal power is combined or divided spatially among the four mixer cards in a waveguide.
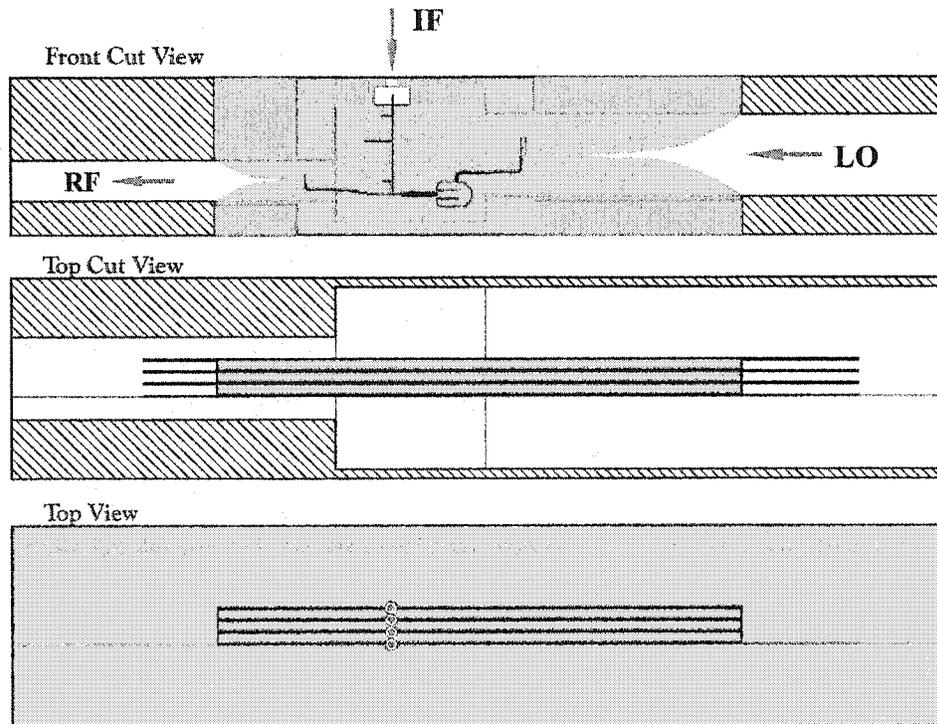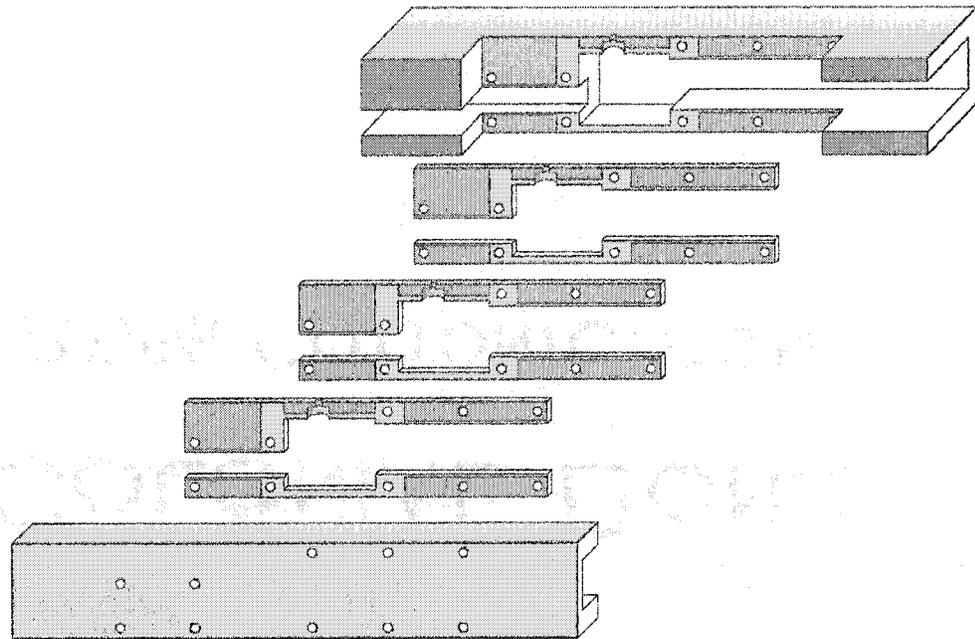
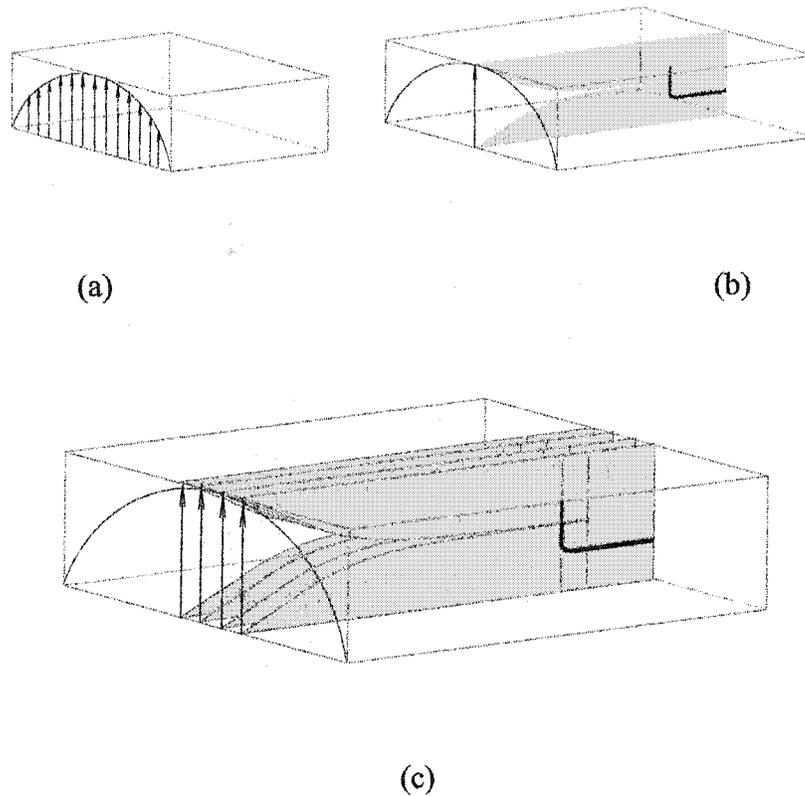Figure 4.11. Structure of spatial waveguide array upconverter

(a)   (b)

(c)

Figure 4.12. The electric field lines for TE_{10}

The spatial waveguide array upconverter is pumped through a standard C-band rectangular waveguide (WR-137). The LO power is spatially divided into the LO port of each mixer unit card at the interface between an air-filled waveguide and the upconverter array and is fed to the microstrip upconverter via waveguide-finline to slot-microstrip transitions. The RF signal of each mixer unit card is spatially combined at the end of the finline with W/b=1 in a standard Ku-band rectangular waveguide (WR-62). The IF signal is applied through coaxial connectors on the top of the waveguide (WR-62). The IF signal is traditionally divided by a 4-split Wilkinson power divider and fed into the IF port of each unit card. The whole card for each mixer unit is realized on the same substrate: dielectric constant $\varepsilon_r = 10.2$ and thickness h=10 mil. Those array cards are symmetric at the middle of WR-137 and WR-62 waveguides.

4.3.2. Performance of Spatial Waveguide Array Upconverter with Single Mixer Unit

For the maximum electric field excitation, the single mixer unit card is inserted in the middle of WR-137 and WR-26 waveguides. The configuration of the spatial waveguide upconverter with signal mixer unit is shown in Figure 4.13.
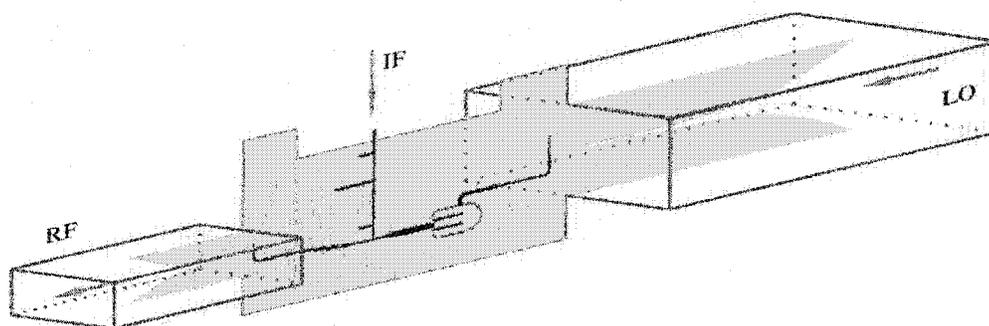

Figure 4.13. Configuration of spatial waveguide upconverter with single mixer unit

A signal generator HEWLETT PACKARD ESG-300A is used as the IF signal source; another signal generator ROHDE & SCHWARZ SMR40 is for LO power source. A power meter ANRITSU ML2438 and a signal analyzer ROHDE & SCHWARZ FSIQ40 are used for the upconverter measurements. The cable losses at RF, IF and LO frequencies are determined using a calibration approach and are de-embedded from the measured data. The other additional losses of two WR137-coaxial and WR26-coaxial transitions and IF launching to microstrip are briefly estimated as 0.3dB.
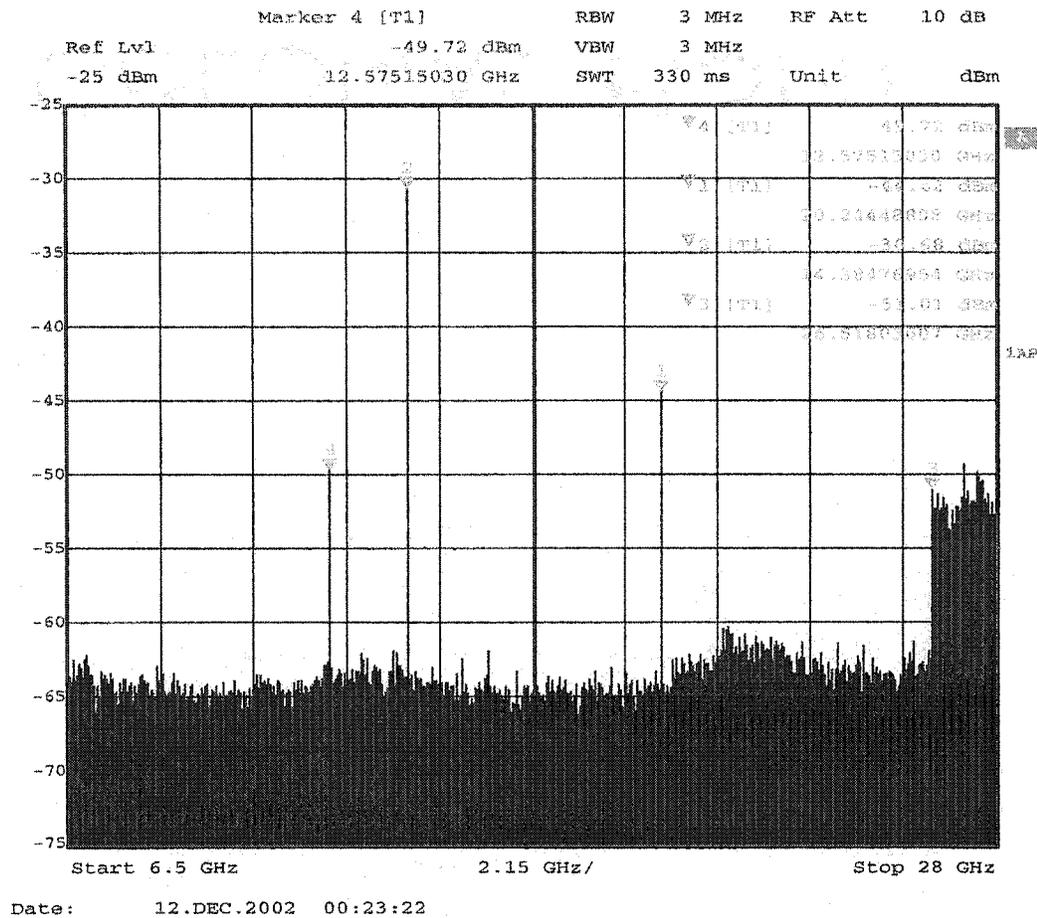
Figure 4.14 Measured output spectrums of the upconverter with single mixer unit.

Figure 4.14 shows the measured out signal spectrum at the RF port, where the LO signal is 6.75 GHz with 8.5 dBm power injected at the LO port, and the IF signal is 900 MHz with –20 dBm power applied at the IF port. As can be seen, there are only three components that we can read. The marker 2 is the RF frequency, which is 14.4($2f_{LO}+f_{IF}$) GHz at –30.68 dBm. Based on a known IF input power level of –20 dBm and a total additional loss of -2 dBm, the conversion loss is only –8.68 dB in this module. The marker 4 is the image response, which is 12.62 ($2f_{LO}$-f_{IF}) GHz with –49.72 dBm. There is a 19.04 dB rejection between RF and image signals. It is obvious that a good suppression

of the image signal can significantly reduce the distortion of the RF signal. The marker 1 is the third-order LO harmonic of 20.25 GHz with –44.42 dBm, and it is 52.92dBc much below the LO signal. In addition, the second-order LO harmonic and all even order (2,2) spurious response cannot be seen. And also, a high LO-to-RF isolation can be anticipated due to the inherent character of the proposed spatial array upconverter structure in which WR-137 waveguide is for LO and WR-62 for RF.
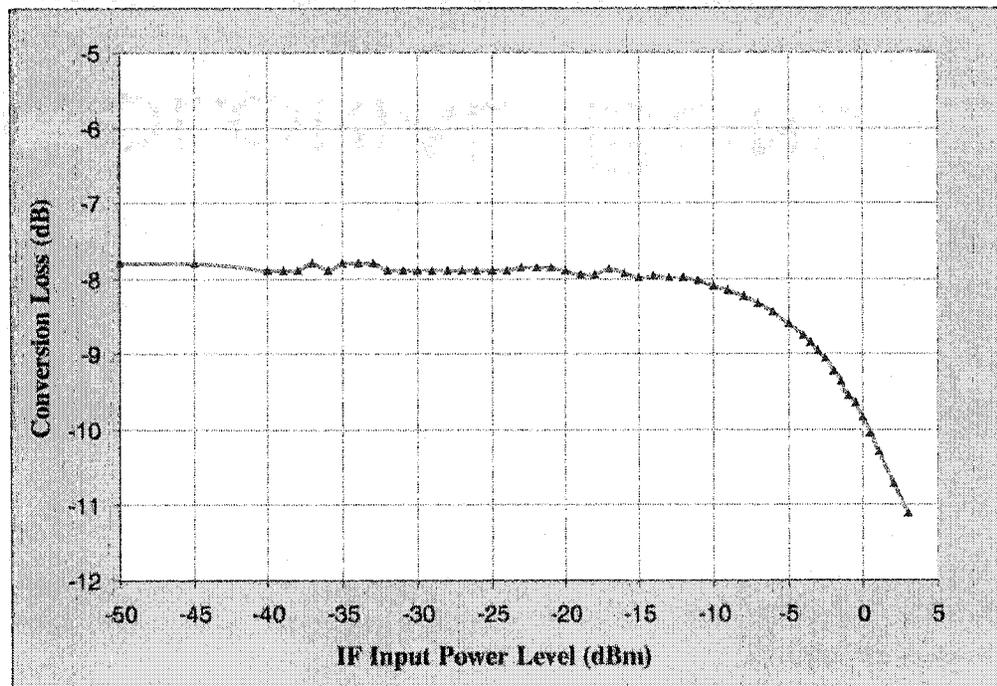

Figure 4.15. Measured conversion loss versus IF input power level.

Figure 4.15 depicts the measured conversion loss of –8 dB ± 0.2 dB when the IF input power is swept from –50 dBm to –10 dBm at IF frequency of 900 MHz and the LO signal is fixed at 6.75 GHz with 8.5 dBm power level. The RF output power versus IF input response curve is shown in Figure 4.16. The 1-dB compression point is higher than

-3 dBm, and more than 40 dB dynamic ranges are obtained. The measured results also show that the developed upconverter has a flat and acceptable conversion loss over a wide input IF dynamic range.
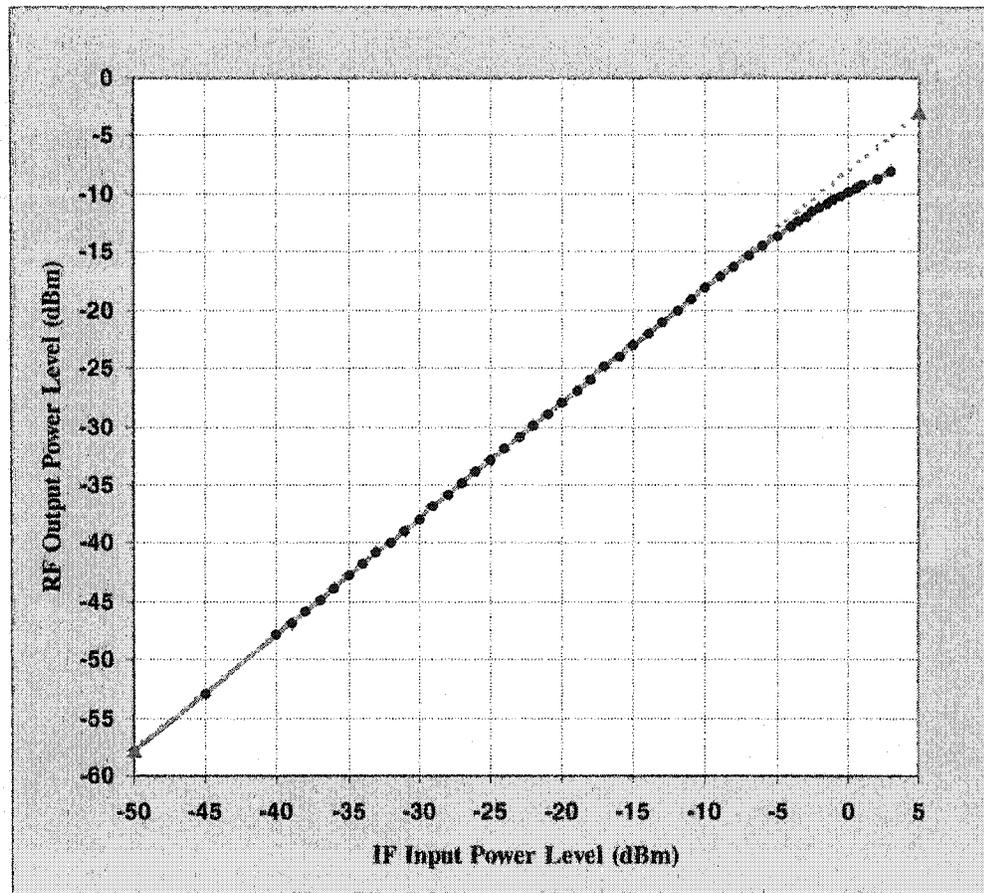

Figure 4.16. Measured RF output versus IF input power level.

Figure 4.17 plots the RF output power and its third-order intermodulation (IM3) power level versus the IF input power. The mixer is excited by two input signal (900MHz and 902MHz) tones having equal magnitude and closely spaced frequencies of 2MHz.

The input third-order intercept point (IP3) is determined to be 11.3 dBm under the 8.5 dBm LO driving at a fixed LO of 6.75 GHz.
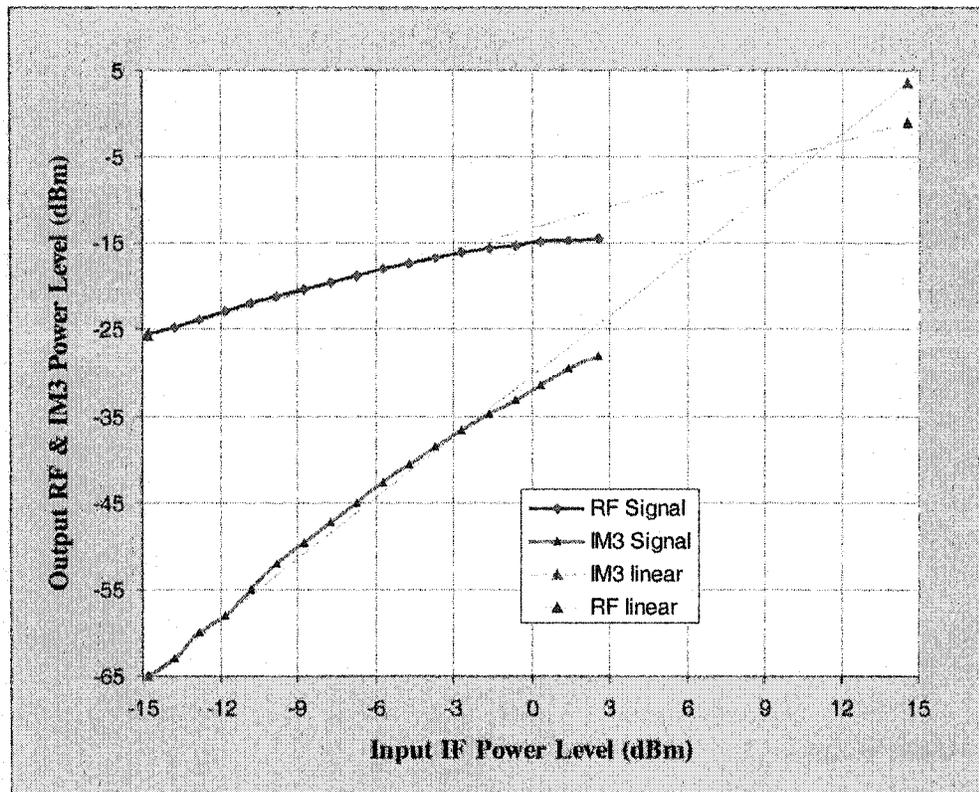

Figure 4.17. Measured output RF & IM3 power versus IF input power level.

Figure 4.18 shows the measured conversion loss versus IF input frequency, when the IF input frequency is swept from 400 MHz to 1000MHz and the LO signal is fixed at 6.75 GHz with 8.5 dBm. As can be seen, the conversion loss is less than 10 dB over an IF frequency range of 400~1000 MHz.
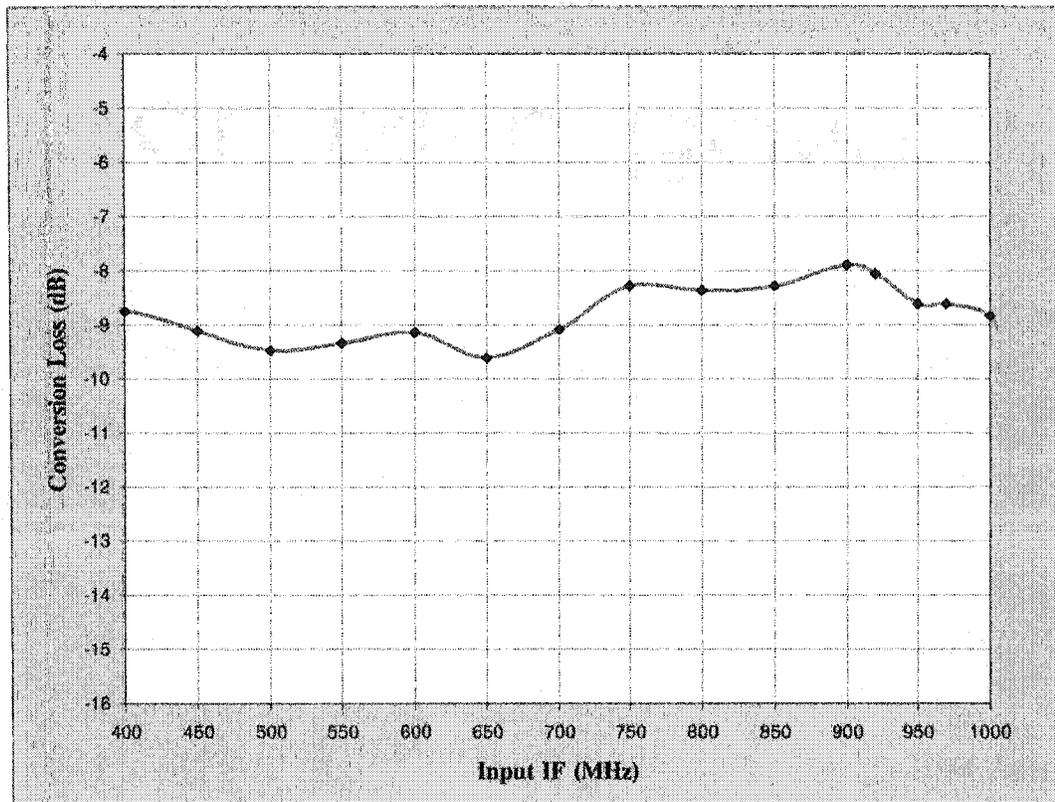
Figure 4.18. Measured conversion loss versus IF input frequency.

4.3.3. Performance of Spatial Array Upconverter with Four Mixer Units

After we have successfully obtained very good performances in the spatial waveguide upconverter with one mixer unit card, the four mixer unit cards are mounted in an array form inside the waveguide. There is 90mil spacing from card to card. The configuration of spatial waveguide array upconverter with four mixer units and the photo of the physical module are shown in Figure 4.19.
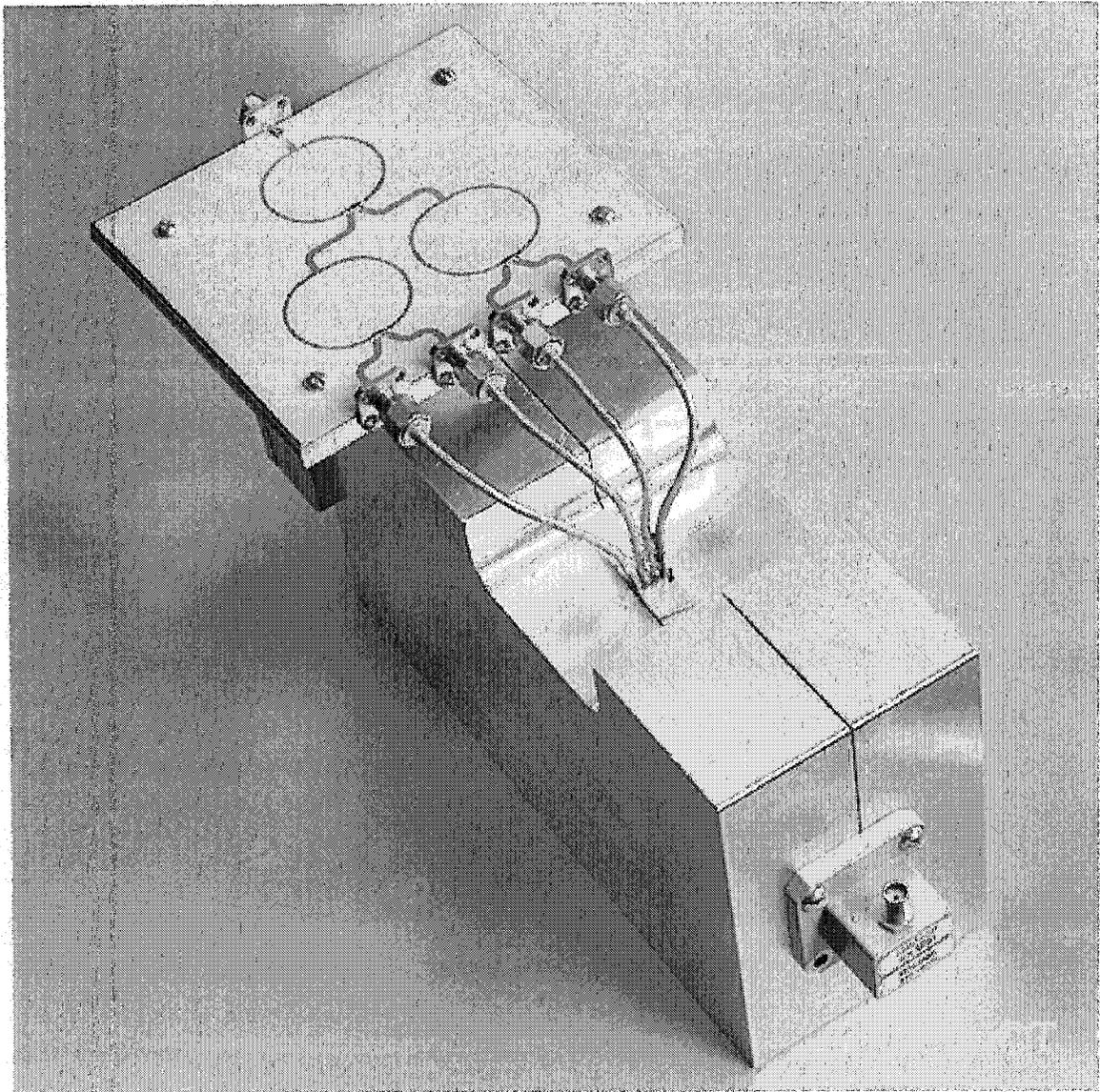
Figure 4.19. Configuration of spatial waveguide upconverter with four mixer units
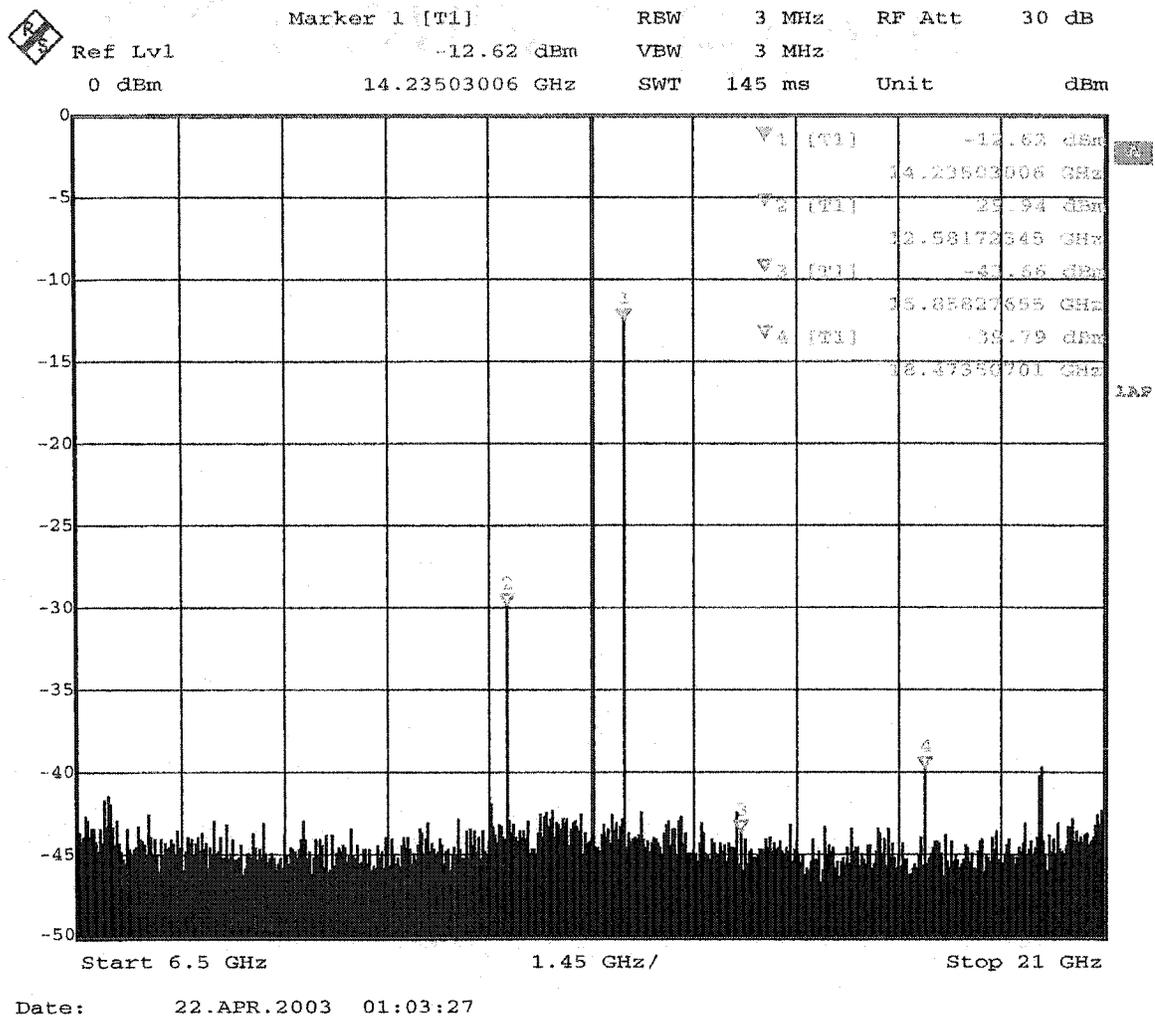
Figure 4.20 Measured output spectrum of the upconverter with four mixer units.

Figure 4.20 shows the measured output signal spectrum at the RF port, where the LO signal is 6.70 GHz with 15.0 dBm power injected at the LO port, and the IF signal is 820 MHz with 0 dBm power applied at the IF port through a four-split Wilkinson power divider. With the measured spectrum, it can be seen that there are only four components that we obviously read at RF frequency of 14.22 GHz ($2f_{LO}+f_{IF}$), image frequency of 12.58 GHz ($2f_{LO}-f_{IF}$), the third-order LO harmonic of 20.1GHz ($3f_{LO}$) and the harmonic 18.46 GHz ($3f_{LO}-2f_{IF}$). The image rejection is larger than 17 dB and the third-order LO

harmonic suppression is 55 dBc below LO signal power. Obviously, the second LO harmonic and some spurious responses are well suppressed in the spatial waveguide array upconverter. In addition, the LO-to-RF isolation is no doubt extremely high (the measured value is higher than 87 dBc) due to the both the SH mixer design and the special structure: different waveguide sections (WR-137 and WR62) for LO and RF paths.
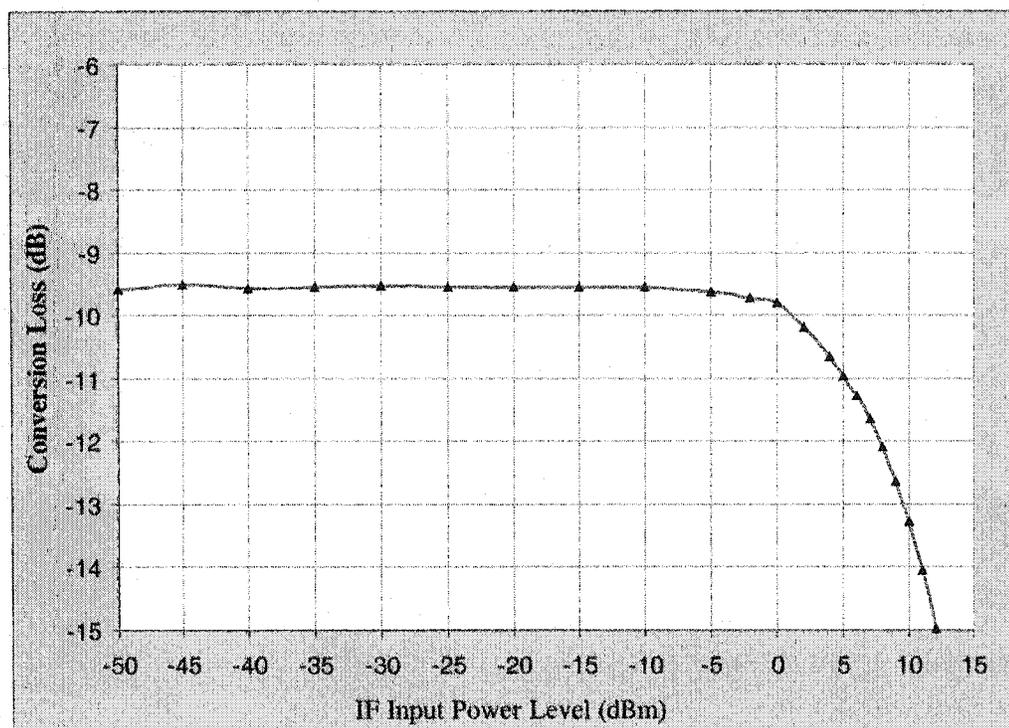
Figure 4.21. Measured conversion loss versus IF input power level.

Figure 4.21 depicts measured conversion loss versus the IF input power level for the spatial waveguide array upconverter with four mixer units. When the IF frequency is set to 820 MHz and the LO signal is fixed at 6.70 GHz with 15.0 dBm power level, the measured conversion loss is around −10 dB. This conversion loss is 1.5 dB high than the single mixer unit upconverter. The reason might be from the radiation due to gaps on the top/bottom of the end of waveguide. That happens at the both sides of LO and RF ports.

Another possibility is that the non-uniform electric field of TE$_{10}$ mode creates different LO power condition for each card. The input 1-dB compression point is higher than 3 dBm. There is a 6dB improvement as compared with the one mixer unit. When the IF input power is swept from −50 dBm to 0 dBm, the conversion loss are almost a constant. The RF output power versus IF input response curve is shown in Figure 4.22. It also displays a very good linearity and higher 1-dB compression point. So, the measured results explain why the spatial waveguide array upconverter can provide enhanced RF efficiency by coupling a number of components into beams in free space so that the spatial upconverter has a higher dynamic range at input port and a larger output power at output port.
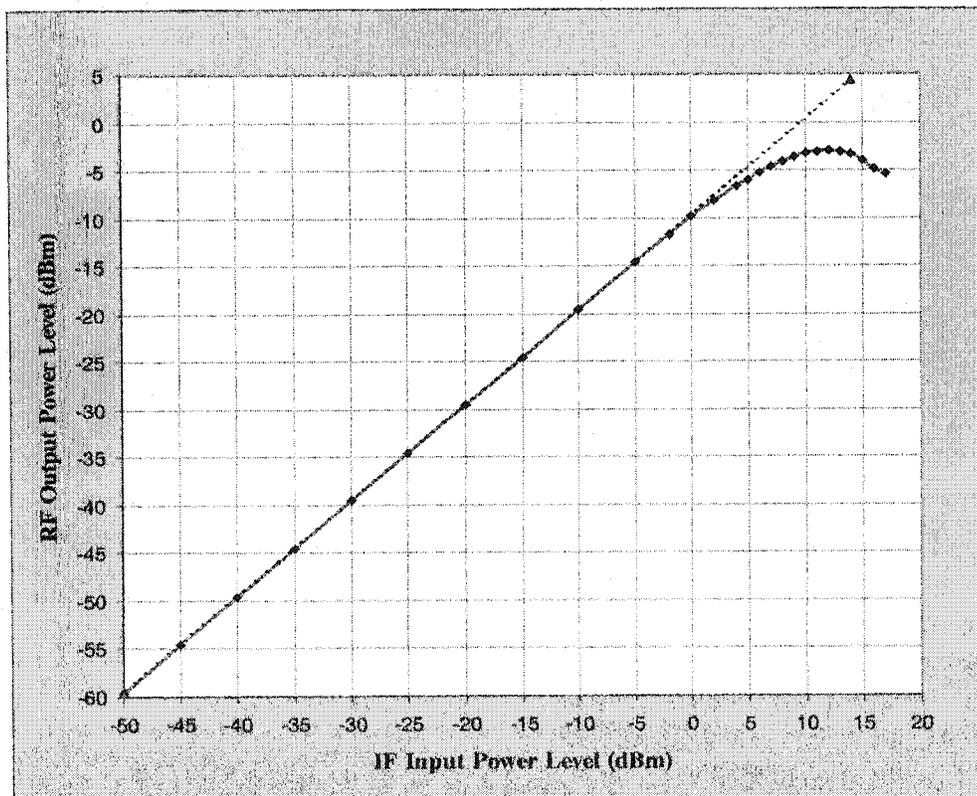
Figure 4.22. The RF output power versus IF input power.
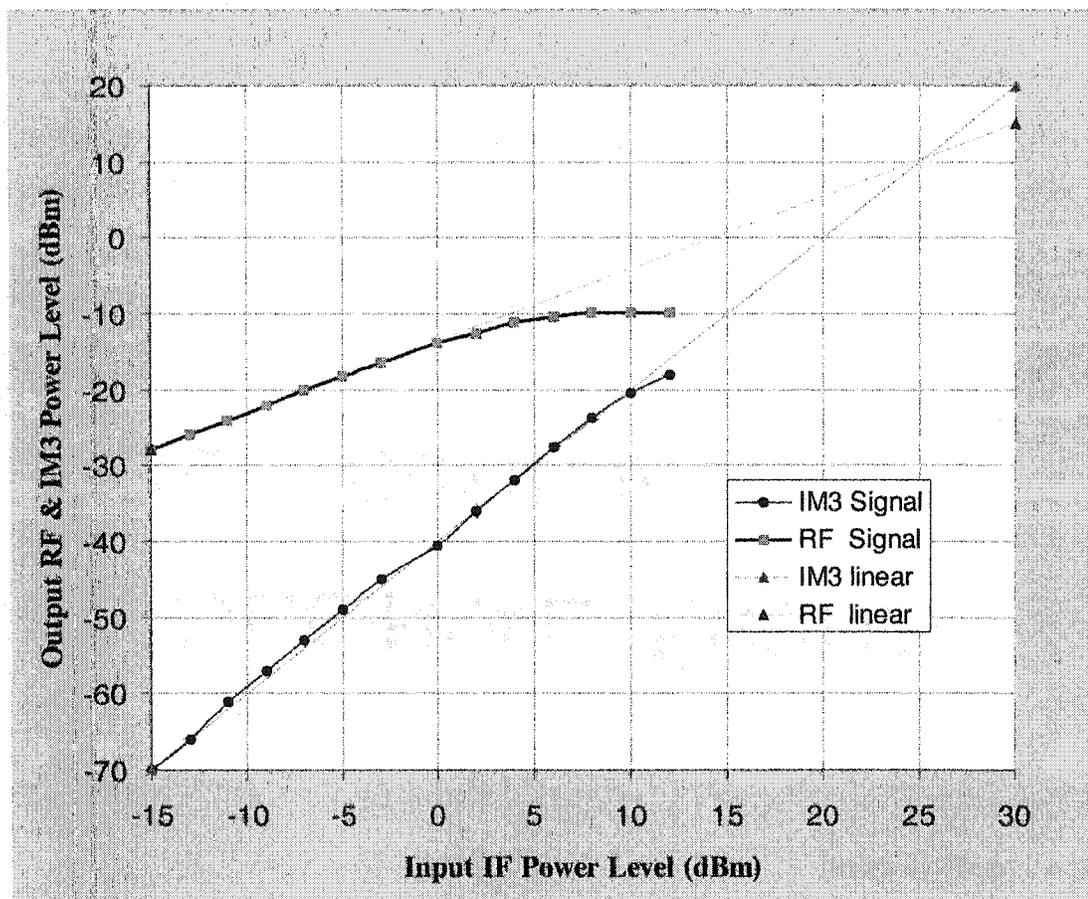
Figure 4.23. The measurement of third-order intermodulation (IM3) point

Figure 4.23 plots the RF output power and its third-order intermodulation (IM3) power level versus the IF input power. The upconverter is excited by two input signal tones (820 MHz and 822 MHz) having equal magnitude and closely spaced frequencies of 2 MHz. The third-order intercept point (IP3) is determined to be 25 dBm under the 15.0 dBm LO driving at a fixed LO of 6.70 GHz. The IP3 point is 14 dB higher than the single mixer unit upconverter.
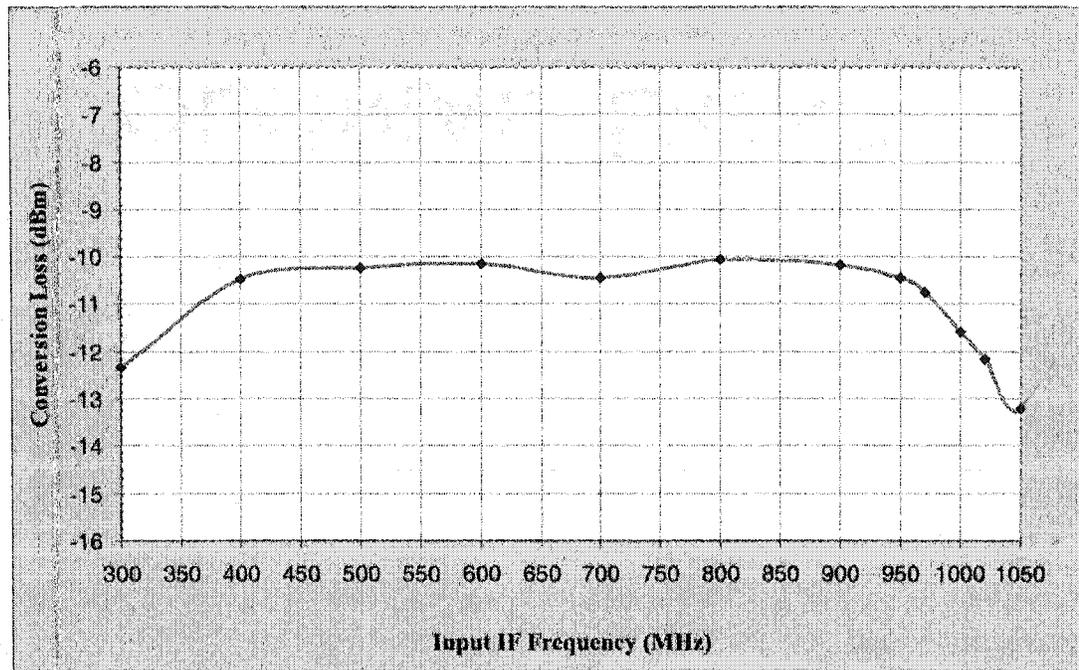
Figure 4.24. Measured conversion loss versus IF input power level with 4 units.

Figure 4.24 shows the measured conversion loss versus IF input frequency, when the IF input frequency is swept from 300 MHz to 1050MHz and the LO signal is fixed at 6.70 GHz with 15.0 dBm power level. As can be seen, the conversion loss is less than 10.5 dB over a large input IF frequency bandwidth of 400~950 MHz. It is also shown that the conversion loss variation is only 0.5 dB over the most of IF bandwidth.

4.4. Conclusion

A novel architecture of spatial waveguide array balanced subharmonic upconverter has been proposed and demonstrated with an attractive structure and performance. It experimentally consists of four mixer unit cards and two different waveguides, WR-137

and WR-62. Each of the unit cards is composed of a balanced subharmonic upconverter, two microstrip-to-slotline transitions and two finline-to-waveguide transitions.

This architecture has shown an impressive performance that features low conversion loss, large bandwidth, extremely high LO-to-RF isolation, excellent suppression capability of even-order harmonics and some spurious signals, higher power combining/dividing efficiency, more power output and less LO power demand over the conventional balanced subharmonic upconverter. These advantages will also be a great benefit for power amplifier and other spatial power combining/dividing components. The proposed spatial waveguide array upconverter could be very useful for base station applications, especially for millimeter-wave front-end transmitter design.

CHAPTER V

CONCLUSIONS AND RECOMMENDATIONS

5. CONCLUSIONS AND RECOMMENDATIONS

Our objective is to realize the first waveguide-based spatial array upconverter in the world with high output power and better signal integrity for the application of millimeter-wave transmitter front–end. The front-end module normally consists of upconverter, RF band-pass filter, LO source and RF power amplifier. To reduce the demand for an excessive power and stable LO source and a high power amplifier at millimeter frequencies, the upconverter is the key component and the core of the module. Therefore, our work is focused on a new architecture of spatial waveguide array upconverter with the attractive spatial combining technology.

To begin with, low-pass and band-pass filters have been analyzed and optimized at a cutoff frequency of 3 GHz and a 10% bandwidth of center frequency 15GHz, respectively, with the insertion loss method. Both filters have demonstrated a good performance in EM simulation. Their in-band low insertion loss and out-of-band high rejection are well suited to our upconverter design.

Then, a balanced subharmonic upconverter that combines the advantages of balanced mixer and subharmonically pumped mixer has been analyzed and optimized for low conversion loss and wide input dynamic range. It is a key building block in this new kind of spatial waveguide array upconverter. The balanced subharmonic upconverter in microstrip format has been realized on 10-mil Duroid 6010LM substrate. It has exhibited a low conversion loss of less than 8 dB over the IF frequency range of 720-1250 MHz when the LO is fixed at the frequency of 6.75 GHz with 8.5 dBm power level. It has also shown a high rejection of second-order LO subharmonic at RF port due to the inherent feature of balanced subharmonic mixer.

Finally, a new upconverter with a wide operating dynamic range and a good power output has been developed. It consists of four balanced subharmonic upconverter unit cards, a WR-137 waveguide and a WR-62 waveguide. On each of the upconverter unit cards, there are a LO waveguide-slotline-microstrip, a microstrip balanced subharmonic upconverter, a RF microstrip-slotline-waveguide. The microstrip-to-slotline transitions have been designed and optimized to have a good mode conversion and impedance transformer by using a commercial 2-D simulator. The finline-to-waveguide transitions have well been designed in WR-137 and WR-62 waveguides, respectively, with low return loss by using a commercial full-wave simulator.

To verify our design approach and to make this proof of concept, the spatial waveguide array upconverter with single unit card has firstly been fabricated. This spatial waveguide upconverter has demonstrated some unparallel advantages: a flat conversion loss of 7.8~9.6 dB over a wide IF bandwidth of 400~1000 MHz driven by a subharmonic LO source of 6.75 GHz and very high isolations between ports and high rejections of some LO/RF harmonics and mixing spurious responses. After that, the spatial waveguide array upconverter with four unit cards have been developed and built. The proposed architecture has experimentally achieved an impressive performance that features low conversion loss, less than 10.5 dB over a large input IF frequency range of 400~950 MHz. It has exhibited a large dynamic input/output range (more than 50 dB) and higher linearity: the input 1-dB compression point of higher than 3.0 dBm, the input third-order intercept point (IP3) of higher than 25.0 dBm under the 15.0 dBm LO driving at a fixed LO of 6.70 GHz. It has also demonstrated 78 dB isolation between LO-to-RF at the LO frequencies, 17 dB suppression of image signal, excellent suppression capability of all even-order harmonics and some other spurious signals and higher power combining efficiency.

Considering the less dependence on fabrication and electric tolerance, our proposed spatial waveguide array upconverter has been realized at Ku-band. However, our design approach can be applied in the development of a millimeter-wave spatial waveguide array upconverter. In addition, dispersion and material loss have to be taken into account in the application of millimeter-wave frequency. In the meanwhile, we should consider the flexibility of substrates that can be mounted in waveguides very well. Therefore, we should choose an adequate substrate when developing spatial waveguide array upconverter in millimeter-wave frequencies.

As known, a remarkable advantage of using such a spatial power combining architecture is that the insertion loss usually does not increase by increasing the number of 2D array of unit cards. To have a higher power output in the spatial waveguide array upconverter, a number (more than 4) of unit cards can be further combined in a waveguide. However, the number might be limited due to the non-uniform TE_{10} modal electric field profile across the waveguide. To increase the number of unit cards in the waveguide, an oversized combiner has been developed to accommodate more units [15]. In this case, both TE_{10} and TE_{20} modes can propagate at a particular operating frequency. By using a symmetric loading of the structure, modes of odd symmetry such as TE_{20} mode can effectively be suppressed. Recently, a TEM waveguide using uniplanar compact electromagnetic bandgap structure has been presented [7]. This compact structure realizes a magnetic surface in the stopband and it is used to replace the two bilateral waveguide walls so to provide a magnetic boundary condition. In this way, the TEM modal condition is satisfied in the rectangular waveguide, and a relatively uniform field distribution along the cross section can be anticipated. With the aid of the alternative solutions, it will no doubt be achieved for a more attractive structure of spatial waveguide array upconverter with higher output power and wider input dynamic range in the oversized or TEM waveguide, provided a careful attention would be paid to the electromagnetic design of the structure.

REFERENCES

[1] J. Harvey, E.R. Brown, D.B. Rutledge, R.A. York. Spatial Power Combining for High-Power Transmitters. Microwave, December 2000.

[2] Stephen A. Maas, Microwave Mixers. 1993

[3] David M. Pozar, Microwave Engineering, John Wiley & Sons Inc., 1998

[4] Huifang Gu, Ke Wu. "Uniplaner Architecture of Broadband Bananced Subharmonically Pumped Mixer".

[5] N. S. Cheng, A. Alexanian, M. G. Case, and R. A. York, "20 Watt Spatial Power Combiner in Waveguide," *IEEE MTT-S International Microwave Symposium Digest*, Baltimore, MD, USA, Jun 8-12 1998, pp. 1457-1460.

[6] N. S. Cheng, A. Alexanian, M. G. Case, and R. A. York, "40-W CW Broad-band Spatial Power Combiner Using Dense Finline Arrays," *IEEE Trans. Microwave Theory and Tech.*, vol. 47, pp. 1070-1076, July 199.

[7] Mekki Belaid, Ke Wu, "Spatial Power Amplifier Using Passive and Active TEM Waveguide Concept." *IEEE Trans. Microwave Theory and Tech.*

[8] Cohn, S.B., "Slotline on a Dielectrate," IEEE Trans. Microwave Theory Tech., Vol. MTT-17, No. 10, October 1969.

[9] Hoffmann, R.K., and J. Siegl, "Microstrip-Slot Coupler Design-Part I: S-Parameters of Uncompensated and Compensated Couplers," , "Microstrip-Slot Coupler Design-

Part II: Practical Design Aspects," IEEE Trans. Microwave Theory Tech., Vol. MTT-30, No. 8, August 1982.

[10] Kitazawa, T., and R. Mittar, "Analysis of Asymmetric Coupled Striplines," IEEE Trans., Vol. MTT-33, 1985, pp.643-646.

[11] Qian, Y., and E. Yamashita, "Characterization of Picosecond Pulse Crosstalk Between Coupled Microstrip Lines with Arbitrary Conductor Width," IEEE Trans., Vol. MTT-25, 1977, pp. 726-729.

[12] Knorr, J. B., and K. D. Kuchler, "Analysis of Coupled Slots and Coplaner Strips and Dielectric Substrate," IEEE Trans., Vol. MTT-23, 1975, pp. 541-548.

[13] Cohn, S. B., "Waveguide-to-Coaxial-Line Junctions," Proc. IRE, September 1947, pp. 920-926.

[14] Gardiol, F., Introduction to Microwaves, Artech House, Norwood, MA, 1984.

[15] L. Y. V. Chen, and R.A. York, "Development of K-Band Spatial Combiner using Active Array Modules in an Oversized Rectangular Waveguide," IEEE MTT-S International Microwave Symposium Digest. Boson, MA, USA, June 11-16 2000, pp 821-824.